Atmospheric Research 338 (2026) 109001

Contents lists available at ScienceDirect

Atmospheric Research

journal homepage: www.elsevier.com/locate/atmosres

Increased early Spring extratropical cyclone peaks over the Western North Pacific after 2000 associated with enhanced baroclinicity and Regime-shift-related background-state changes

Yeomin Jeong [a], Jong-Min Kim [b], Sera Jo [c], Eung-Sup Kim [c], So-Hee Kim [d], Cheol-Hee Kim [a,b], Joong-Bae Ahn [a,*], Hyo-Jung Lee [a,b,*]

[a] *Institute of Environmental Studies, Pusan National University, Busan 46241, Republic of Korea*
[b] *Department of Atmospheric Sciences, Pusan National University, Busan 46241, Republic of Korea*
[c] *Climate Change Assessment Division, National Institute of Agricultural Sciences, Wanju 55365, Republic of Korea*
[d] *Division of Environmental Science and Engineering, Pohang University of Science and Technology, Pohang, Republic of Korea*

ARTICLE INFO

Keywords:
Extratropical cyclone
Western Pacific pattern
Pacific Decadal Oscillation
Okhotsk Sea-ice
Baroclinicity

ABSTRACT

We examined the significant increase in extratropical cyclone (ETC) peak occurrences over the marginal seas of the Western North Pacific and their vicinities (ETC-peak area) during early spring after 2000, and analyzed the contributing factors. We defined the pre- and post-2000 periods to represent the two decades before and after 2000, respectively. A composite analysis comparing the two periods indicated that a negative sea level pressure (SLP) anomaly was located over the ETC-peak area during the post-2000 period, creating favorable conditions for enhanced cyclone development.

Particularly, the increase in negative SLP anomaly over the northwestern sector, together with positive SLP anomalies strengthening in the North Pacific south of the Aleutian Islands, led to an increased SLP gradient along the corridor from the southeastern coast of the Japan archipelago to the Kamchatka Peninsula. This enhanced gradient facilitated the advection of warm, moist air from the southeast, resulting in the increased temperature gradient and, thereby, enhancing baroclinicity and westward tilting of geopotential height, and creating a favorable environment for cyclone development over the region, which was not observed during the pre-2000 period. We further examined correlations between various large-scale climate indices and the ETC-peak frequency. In contrast, during the post-2000 period, the ETC-peak occurrence exhibited significant correlations with the Western Pacific (WP) and Pacific Decadal Oscillation (PDO) indices. Specifically, an increase (decrease) in ETC-peak occurrence is associated with the positive (negative) phase of the WP and the negative (positive) phase of the PDO. While the WP index does not exhibit a long-term trend, the PDO index showed a clear decreasing trend with negative values in most years during the post-2000. Therefore, although the WP appears to have influenced interannual variability of ETC activity over the region, the PDO-driven background-state changes likely played a substantial role in the observed increase in ETC-Peak occurrence during the post-2000 period.

1. Introduction

The region encompassing the marginal seas of the northwestern Pacific, such as the Sea of Okhotsk, East Sea/Sea of Japan, and Yellow Sea, and their adjacent areas, including the Kamchatka Peninsula, Korean Peninsula, Japanese Archipelago, Kuril Islands, and the region of the Kuroshio current, represents the interface between the eastern Eurasian continent and the northwestern Pacific (Fig. S1). This region is characterized by strong seasonal monsoonal events (e.g., Lau and Li, 1984). That is, during the cold seasons, relatively cold, dry air masses originating from the Eurasian continent interact with warm, moist air influenced by the seawater of the northwestern Pacific, producing strong baroclinicity. Consequently, the generation and development of extratropical cyclones (ETCs) are active in this area. Also, heat and moisture fluxes released into the atmosphere through ocean–atmosphere interactions in this region are crucial for the global atmospheric energy and moisture budgets. From an energy perspective, the vigorous conversion of eddy potential energy into eddy and zonal-mean kinetic

* Corresponding authors at: Institute of Environmental Studies, Pusan National University, Busan 46241, Republic of Korea.
E-mail addresses: jbahn@pusan.ac.kr (J.-B. Ahn), hyojung@pusan.ac.kr (H.-J. Lee).

https://doi.org/10.1016/j.atmosres.2026.109001
Received 23 November 2025; Received in revised form 4 April 2026; Accepted 5 April 2026
Available online 8 April 2026
0169-8095/

energies leads to the presence of one of the strongest upper-tropospheric jet streams in the Northern Hemisphere, the East Asian jet (e.g., Lorenz, 1955). On the other hand, during the warm season, the influence of the North Pacific High (NPH) often results in extreme heat events. In early summer, the northward expansion of the NPH establishes a Baiu/Changma/Meiyu stagnant front over the region, producing a prolonged rainy season accompanied by persistent heavy precipitation, sometimes lasting for approximately a month depending on the location (e.g., Hong and Ahn, 2015). From late summer to autumn, typhoons that develop over the Western North Pacific (WNP) often pass through the region or undergo an extratropical transition, occasionally causing substantial damage (e.g., Emanuel, 2005). Furthermore, during spring, ETCs originating from inland regions, such as China and Mongolia, frequently transport Asian dust, affecting the region (e.g., Chun et al., 2001). Thus, this meteorologically dynamic zone exhibits a wide range of atmospheric phenomena throughout the year and holds substantial climatological significance.

In early spring, in particular, this region experiences highly variable weather owing to the combined effects of several contrasting air masses and forcings: warm and dry migrating anticyclones originating from the Yangtze River basin; cold and dry air intruding southward from Siberia/Mongolia; cold and wet air masses sourced from the Sea of Okhotsk and the Kamchatka region; and hot and humid air extending from the WNP (Kim and Ahn, 2024). Spring is a transitional period marked by the retreat of continental cold air masses and the expansion of warm marine air masses from a large-scale perspective, during which ETC passages across the region reach their climatological maximum (e.g., Fu et al., 2014; Gao et al., 2025). ETC activity during spring is of great socioeconomic importance, particularly for agriculture and hydrology, to countries within and adjacent to this region (Okajima et al., 2025). ETCs that develop or pass through this region often intensify into strong systems accompanied by heavy precipitation and severe winds in spring. Fu et al. (2014) argued that this tendency is driven by pronounced temperature gradients between the continent and ocean as well as vigorous air–sea interactions. Recently, Okajima et al. (2025) investigated the mechanisms responsible for the springtime peak in the cyclogenesis of so-called Kuroshio cyclones, which form over southern China and the East China Sea and subsequently propagate along the Kuroshio Current.

Zhang et al. (2022) investigated explosive ETCs, which are defined as cyclones with a central pressure deepening of at least 24 hPa within 24 h, across the East Sea/Sea of Japan and the Kuroshio Extension. Their findings indicate that ETCs over the Kuroshio Extension peak in early spring (March) and exhibit higher deepening rates, lower central pressures, and longer lifespans than those over the East Sea/Sea of Japan. Yamashita et al. (2012) examined the activity of an explosive ETC around the East Sea/Sea of Japan, and found that explosive cyclone tracks concentrate around the Kuroshio Current off the Pacific coast of Japan and the East Sea/Sea of Japan when the East Asian winter monsoon is strong. Gao et al. (2022) compared the initial development of explosive and nonexplosive ETCs off the East Asian coast. The study illustrated that despite the importance of diabatic processes in the deepening of mid-latitude cyclones emphasized by many studies, the potential vorticity intrusion dominated by cold air masses is the key cause of explosive cyclogenesis in this region. Zhang et al. (2019) investigated the interannual variability of cyclones generated over the eastern Asian continent and that pass over the Yellow, Bohai, and East China Seas (YBE cyclones) in spring for the period 1979–2017 and found that the number of YBE cyclones exhibited significant interannual variability over a period of 4–5 years. From the analysis, they argued that rapidly developing cyclones are related to sea surface temperature anomalies and atmospheric baroclinicity from Lake Baikal to the East Sea/Sea of Japan, and that slowly developing cyclones seem to be related to the North Atlantic Oscillation (NAO) in the preceding winter. Meanwhile, Kuwano-Yoshida and Asuma (2008) conducted numerical simulations of explosive ETCs occurring in the Northwest Pacific using the MM5 model. Through these experiments, they demonstrated that the interaction between strong low-level baroclinicity and large-scale latent heat release from the ocean is essential for the rapid intensification of these cyclones. Overall, previous studies indicate that the development of both explosive and non-explosive ETCs over the region is primarily governed by a combination of enhanced low-level baroclinicity, air–sea heat and moisture fluxes, upper-level potential vorticity intrusions associated with cold-air outbreaks, and large-scale modes of variability such as the North Atlantic Oscillation.

Owing to the availability of satellite passive microwave remote-sensing data, variations in the extent of sea ice have been relatively well documented since 1979 (Vihma, 2014). Numerous studies have discussed the relationship between sea ice and various meteorological and climatic variabilities in the Northern Hemisphere (e.g., Budikova, 2009; Bader et al., 2011; Vihma, 2014). Several studies suggested that sea ice loss in the Sea of Okhotsk in winter and spring results in increased cyclogenesis, which strengthens the North Pacific storm track (Kamae et al., 2023; Kamae and Yokota, 2025; Mesquita et al., 2013). Honda et al. (1996, 1999) suggested that sea ice anomalies in the Sea of Okhotsk generate a stationary wave train response with far-reaching downstream effects. Screen (2013) also proposed that the prevailing low over the North Pacific, together with sea ice loss in Hudson Bay and the Labrador Sea, generates a stationary wave train. Wu et al. (2013) insisted that the wave train subsequently induces a prevailing low over the Northeast Atlantic and British Isles from May to June. Overall, these studies demonstrate that sea-ice variability in the Sea of Okhotsk can exert substantial influences on the climate of not only the Sea of Okhotsk and its surrounding regions but also other high-latitude areas of the Northern Hemisphere through planetary-wave teleconnections.

Gao et al. (2025) recently showed a weakening trend of bomb cyclones in the North Pacific since the beginning of the 21st century in terms of significant reductions in maximum near-surface wind speeds, increases in minimum sea level pressure, and slower deepening rates. On the other hand, Hsu et al. (2025) argued that wintertime eddy kinetic energy and baroclinicity over the North Pacific midlatitudes have increased, leading to a strengthening of the storm track, enhanced extratropical cyclone activity, an increase in cyclone frequency along certain tracks, and even a rise in the occurrence of bomb cyclones. However, these seemingly contradictory results can coexist spatially, characterized by a weakening of bomb cyclones in the midlatitudes (East Sea/Sea of Japan, 30–45°N) and a concurrent intensification of storm-track activity at higher latitudes (the Sea of Okhotsk and the Bering Sea). Recent studies consistently indicate that extratropical cyclone activity in wintertime over the region has undergone significant structural changes, characterized primarily by a poleward shift of the storm track, alongside regionally dependent changes in intensity, frequency, and dynamical characteristics. However, relatively few attempts have been made to understand the ETC changes in this region from a large-scale perspective. Xie et al. (2020) analyzed the impacts of five large-scale patterns—the El Niño Southern Oscillation (ENSO), Western Pacific (WP), NAO, Pacific–North America (PNA), and Pacific Decadal Oscillation (PDO) patterns—on winter ETC track density. Their results indicated that ETC track density exhibited significant differences between the periods 1979–1998 and 1999–2018, and that among the five patterns, the WP, NAO, and PDO patterns seemed to contribute to the variability in ETC track density, with the negative phases of these patterns generally associated with higher track density. However, their analysis was limited to statistical correlations between the five indices and wintertime storm track density, without addressing the underlying dynamical mechanisms.

Although spring is a season of enhanced extratropical cyclone activity over the marginal seas of the WNP due to increased low-level baroclinicity and greater jet variability (Okajima et al., 2025), relatively little attention has been paid to changes in springtime ETCs in the region in association with decadal-to-interdecadal climate variability. In particular, although the frequency of ETCs passing through the region has increased significantly in recent early springs (Supplementary Fig. 1), this change has not been adequately examined. In this study, we investigated changes in springtime number of ETC peaks over the marginal seas of the WNP and their surrounding regions over the past four decades. Considering that transitions of the PDO to its negative phase (e.g., Newman et al., 2016) and the Atlantic multi-decadal oscillation (AMO) to its positive phase (e.g., Enfield and Cid-Serrano, 2010) occurred almost simultaneously around 2000 (e.g., Hu et al., 2011), along with ongoing global warming, we divided the analysis period into two 20-year periods (pre- and post-2000) and examined changes in ETC peaks to analyze possible dynamical mechanisms and contributing factors. The datasets and methodologies employed in this study are described in Section 2. Section 3 presents the main results. Section 4 provides the conclusions, followed by a discussion of the implications and limitations of the study.

2. Data and methods

2.1. Definition of ETCs

The detection and tracking algorithm proposed by Hodges (1994, 1995, 1999) was used to identify ETCs over East Asia. Relative vorticity at 850 hPa was used instead of Sea Level Pressure (SLP), as SLP-based methods are less effective during early system development and can introduce significant errors in regions with complex terrain (Sinclair, 1997; Hodges, 1999). Relative vorticity was calculated from the 6-hourly wind components (u, v) of the NCEP/DOE Reanalysis 2 (NCEP R2) dataset for 1981–2020. To reduce the influence of planetary-scale waves, spectral components with wave numbers less than five were removed.

The connected-component labeling algorithm (Rosenfeld and Kak, 1976) was applied to identify contiguous relative vorticity regions, with the local maximum in each region defined as the ETC center. Identified centers were tracked every 6 h. Systems were classified as ETCs if they formed north of 25°N, had a lifetime of at least two days, traveled more than 1000 km, and exhibited a central intensity greater than 1.0×10^{-5} s^{-1} (Hoskins and Hodges, 2002; Lee et al., 2020; Kim and Ahn, 2024).

Because each ETC had different genesis locations and trajectories, the coordinate of the absolute maximum central intensity during its entire lifetime was defined as the unique representative point for spatial distribution and further analyses. By defining only one such peak coordinate for an individual cyclone's entire life cycle, we ensured that each cyclone was counted only once in the frequency statistics, thereby avoiding potential biases caused by slow-moving or long-duration cyclones. This study adopts the ETC detection and tracking scheme as implemented in Kim and Ahn (2024) to ensure methodological robustness and consistency.

2.2. Data and analysis period

This study investigated large-scale climate variability associated with ETCs over East Asia using multiple reanalysis and observational datasets. For atmospheric variables, we used the NCEP/DOE Reanalysis 2 (NCEP R2) dataset, which provides a spatial resolution of $2.5^\circ \times 2.5^\circ$ and incorporates an improved data assimilation system compared to the NCEP R1 (Kanamitsu et al., 2002). To ensure stable identification, this resolution was chosen to effectively capture synoptic-scale cyclone structures while filtering out potential small-scale noise during the tracking process. Key variables analyzed include SLP, zonal wind (U), meridional wind (V), temperature (T), and geopotential height (Z), specifically utilizing data at representative pressure levels such as 850 hPa, 500 hPa, and 300 hPa. To better resolve thermodynamic structures such as heat fluxes and temperature advection, we additionally employed the fifth-generation atmospheric reanalysis (ERA5) from the European Centre for Medium-Range Weather Forecasts (ECMWF), which provides a grid spacing of $0.25^\circ \times 0.25^\circ$ (Hersbach et al., 2020). Oceanic and sea ice conditions were obtained from the Hadley Centre Sea Ice and Sea Surface Temperature (HadISST) dataset provided by the UK Met Office, with a spatial resolution of $1^\circ \times 1^\circ$. These data were used to represent sea surface temperature (SST) and sea-ice concentration (SIC) variability. The interannual variability of SIC in HadISST is highly consistent with that in ERA5 ($r > 0.98$, $p < 0.01$), indicating that the use of multiple datasets does not affect the results.

The study covers a 40-year period from 1981 to 2020. To focus on interannual variations, anomalies were calculated by removing the 40-year climatological mean and linear trends from the monthly data. For interdecadal comparison, the entire period was partitioned into two distinct 20-year sub-periods: 1981–2000 (hereafter pre-2000) and 2001–2020 (hereafter post-2000). To provide an objective rationale for partitioning the two periods, we conducted multiple changepoint detection analyses, including a sliding *t*-test, the Cumulative Sum (CUSUM) method, and the Moving Standard Deviation (MSDEV). These analyses consistently identified the year 2000 as a statistically significant structural break point ($p = 0.011$), representing a regime shift in the March ETC frequency (Fig. S2). In addition, detailed information regarding the climate indices used in this study is presented in Table 1.

3. Results and discussions

3.1. Composite analysis of ETC-peak and atmospheric patterns

3.1.1. ETC-peak frequency and atmospheric structure changes

Fig. 1 presents the difference in the frequency distribution of ETCs at their peak development (ETC-peak) between pre-2000 and post-2000 over East Asia for each month from February (a) to May (d). The parallelogram shown in Fig. 1b indicates the region where the ETC-peak frequency increased substantially in March (ETC-peak region, hereafter), and Fig. 1e shows the interannual variation of the ETC-peak frequency in that region. Compared to the pre-2000 period, the ETC-peak frequency in the Sea of Okhotsk, including the coastal waters of Korea, Japan, and the Kuril Islands, exhibited a statistically significant increase during March in the post-2000 period (Fig. 1b, e), which tended to decrease in other months (Fig. S3). The regions from southern Japan to the Primorye region of Russia, the Sea of Okhotsk, and the WNP near the Kuril Islands are traditionally areas of active ETC development (Fig. S1). In this study, most of the region encompassing the marginal seas of the northwestern Pacific and their adjacent areas are included in the ETC-peak region.

Before analyzing the cause of the increase in ETC-peak frequency in this region during the post-2000 period compared to the pre-2000 period (Fig. 1e), we first examined the composite SLP for years with a high number of ETC-peaks in March (years exceeding +0.43 standard deviation (STD; corresponding to the upper tertile)) and years with a low number of ETC-peaks (years below −0.43 STD; the lower tertile) in the area (Fig. 2). The left and right panels of Fig. 2 show arithmetic and normalized differences, respectively. Negative anomalies were observed from the western Bering Sea to the Yellow Sea, centered around Sakhalin during the years with a high number of ETC-peak events; whereas positive anomalies were located south of the Aleutian Islands (Fig. 2a). The distribution of normalized SLP is overall similar to Fig. 2a, but the negative anomaly centered around Sakhalin appears more clearly pronounced (Fig. 2b). Considering that early spring is a period when the Aleutian Low and Siberian High still influence the ETC-peak area and the NPH begins to strengthen, this anomaly pattern indicates the weakening of the Aleutian Low and Siberian High, along with the NPH strengthening compared to normal years. In years with high ETC-peaks, the Aleutian Low shifted eastward, whereas the NPH shifted northwestward, relative to normal years. In contrast, in years with low ETC-peaks, positive anomalies were observed from the western Bering Sea to the East Sea/Sea of Japan (Fig. 2c). These characteristic anomaly patterns were also clearly reflected in the normalized SLP anomaly distributions (Fig. 2d). Overall, the similarity in the spatial patterns of

Table 1
Definitions and data sources of the climate index acronyms used in this study.

Index Acronym	Climate Index	Methodology / Definition	Reference
WP	Western Pacific Pattern index	Z500(60°N, 155°E) − Z500(30°N, 155°E) Sign reversed to match the NOAA CPC convention.	Wallace and Gutzler (1981); NOAA CPC
PDO	Pacific Decadal Oscillation index	Time series of the first EOF of monthly SST anomalies over the North Pacific (north of 20°N)	Mantua et al. (1997); NOAA NCEI
ENSO	El Niño–Southern Oscillation index	SST(5°N–5°S, 170°W–120°W)	Trenberth (1997)
IOD	Indian Ocean Dipole index	SST(10°S–10°N, 50°–70°E) − SST(10°S–0°, 90°–110°E)	Saji et al. (1999); BoM
PJ	Pacific–Japan Pattern index	Z850(20°N–25°N, 120°E–130°E) − Z850(30°N–40°N, 135°E–145°E)	Kosaka and Nakamura (2010)
EA/WR	East Atlantic / Western Russia Pattern index	Z500(55°N, 20°E) − Z500 (40°N, 60°E)	Barnston and Livezey (1987); NOAA CPC
AO	Arctic Oscillation index	1st EOF of Z1000 anomalies poleward of 20°N	Thompson and Wallace (1998); NOAA CPC
$EAWM_{SLP}$	East Asian Winter Monsoon (SLP Index)	(2 × SLP(40°N–60°N, 70°E–120°E) − SLP(30°N–50°N, 140°E–170°W) − SLP(20°S–10°N, 110°E–160°E))/2	Wang and Chen (2014)
$EAWM_{U300}$	East Asian Winter Monsoon (U300 Index)	U300(27.5°N–37.5°N, 110°E–170°E) − U300(50°N–60°N, 80°E–140°E)	Jhun and Lee (2004)
$EAWM_{Z500}$	East Asian Winter Monsoon (Z500 Index)	Z500(25°N–45°N, 110°E–145°E)	Wang and He (2012)
EAJSI	East Asian Jet Stream index	U300(30°N–35°N, 120°E–150°E)	Yang et al. (2002)
WPSH	Western Pacific Subtropical High index	Z850(15°N–25°N, 115°E–150°E)	Wang et al. (2013)
ISM	Indian Summer Monsoon index	U850(0–20°N, 40°E–110°E) – U200(0–20°N, 40°E–110°E)	Webster and Yang (1992)
EASM	East Asian Summer Monsoon index	U850(10°N–40°N, 110°E–140°E) – U200(10°N–40°N, 110°E–140°E	Wang and Fan (1999)
OK Sea Ice	Okhotsk Sea Ice Extent index	SIC (50°–62°N, 136°–160°E)	Rayner et al. (2003)
NAT	North Atlantic Tripole Pattern index	SST(5–20°N, 55–15°W) + SST(45–65°N, 40–10°W) − SST(25–45°N, 55–15°W)	Czaja and Frankignoul (2002)

anomalies between the two cases, with opposite signs, suggests a systematic difference between years with high (above +0.43 STD) and low (below −0.43 STD) ETC-peaks (Fig. 2e,f).

To investigate the cause of the ETC-peak increase during the post-2000 period relative to the pre-2000 period, we examined the composite SLP in March for both periods. As shown in Fig. 3, the post-2000 period was characterized by the weakening of the continental high centered over Mongolia–Central Asia and a substantial weakening of the Aleutian Low, compared to the pre-2000 period. Notably, the Aleutian Low weakened and split into eastern and western cores, which shifted to the Gulf of Alaska and the Kamchatka Peninsula, respectively. The reduction in the zonal pressure gradient led to a weakening of the northerly winds over northeastern China, Primorye, and Sakhalin, which could have corresponded to the weakening or earlier termination of the winter monsoon.

The eastward displacement of the Aleutian Low core toward the Sea of Okhotsk, together with the weakening of the continental anticyclone, particularly the negative SLP anomalies over the Okhotsk–Primorsky–Japan–Korea region (Fig. 3c, d), indicates that this area experienced enhanced or more favorable conditions for cyclone development. A pronounced SLP difference gradient was evident from the eastern coast of the Japanese Archipelago to the Kamchatka Peninsula, implying that warm, moist air from lower latitudes was more readily transported northeastward in the lower troposphere, thereby further promoting the development of cyclones. Moreover, the negative anomaly centered over the Sea of Okhotsk and Sakhalin is likely related to the long-term decline in the sea-ice extent and enhanced ice melting in the Sea of Okhotsk over recent decades. This is discussed further in Section 3.2.1.

Fig. 4 shows the differences in the 850-hPa, 500-hPa, and 200-hPa geopotential heights between the post-2000 and pre-2000 periods. A spatial pattern similar to the SLP differences appeared at 850 hPa. It included a negative anomaly centered over the West Siberian Plain, and negative and positive anomalies located south of Sakhalin and the Aleutian Islands, respectively. As illustrated by the normalized differences, pronounced negative anomalies emerged over the ETC-peak region, whereas positive anomalies dominated the south of Sakhalin and the Aleutian Islands. At both 500 and 200 hPa, the locations of the major positive and negative peaks in midlatitudes corresponded closely with those observed in the SLP and 850-hPa fields. In particular, the negative and positive peaks over the West Siberian Plain and the Aleutian Islands exhibited nearly vertically aligned features, indicating equivalent barotropic structures. In contrast, over the ETC-peak area, the negative peak centered over the Okhotsk area tilts westward with height, forming a baroclinic structure (Fig. 5). This suggests that, relative to the pre-2000 period, the geopotential structure in this region became more baroclinic during the post-2000 period, thereby providing a more favorable environment for cyclone development. A more detailed discussion of the dynamical mechanism responsible for the increased baroclinicity in this region is provided in the following subsections and in Section 4 (Discussion).

3.1.2. *Thermal and ocean–atmosphere influences on ETC-peak*

Fig. 6 shows the 850 hPa temperature, 925 hPa temperature advection, and 925 hPa streamlines, and their differences between the post-2000 and pre-2000 periods. The 850 hPa temperature differences indicate positive anomalies extending zonally across East Asia centered over regions north and south of the Sea of Okhotsk to the dateline (Fig. 6g). Meanwhile, the 925 hPa temperature advection differences revealed two factors contributing to the temperature increase over the northwestern Pacific, including the Okhotsk region (Fig. 6g). First, the weakening of the continental anticyclone and Aleutian Low led to enhanced anomalous warm advection in this area. However, this apparent increase in warm advection does not result from an actual strengthening of warm air advection, but primarily from a reduction in cold advection during the post-2000 period relative to the pre-2000 period (Fig. 6e, b). Second, consistent with the SLP differences (Fig. 3c, d), the negative anomalies centered over Primorsky and Sakhalin, together with the positive anomaly south of the Aleutian Islands, strengthened the anomalous southwesterly winds in the region (Fig. 6i), thereby enhancing the advection of warm air (Fig. 6h). Fig. 6i illustrates an aspect of the lower-tropospheric circulation changes over the region extending from the Sea of Okhotsk to the western Bering Sea. The figure indicates the zonal separation of the Aleutian Low center as well as the weakening of the low. The east–west splitting of the Aleutian Low enhanced the cyclonic flow around Sakhalin and strengthened the southerly inflow into the Sea of Okhotsk. This increase in the cyclonic circulation over the Okhotsk region was also linked to the enhancement of warm air advection from the south, which may have contributed to a

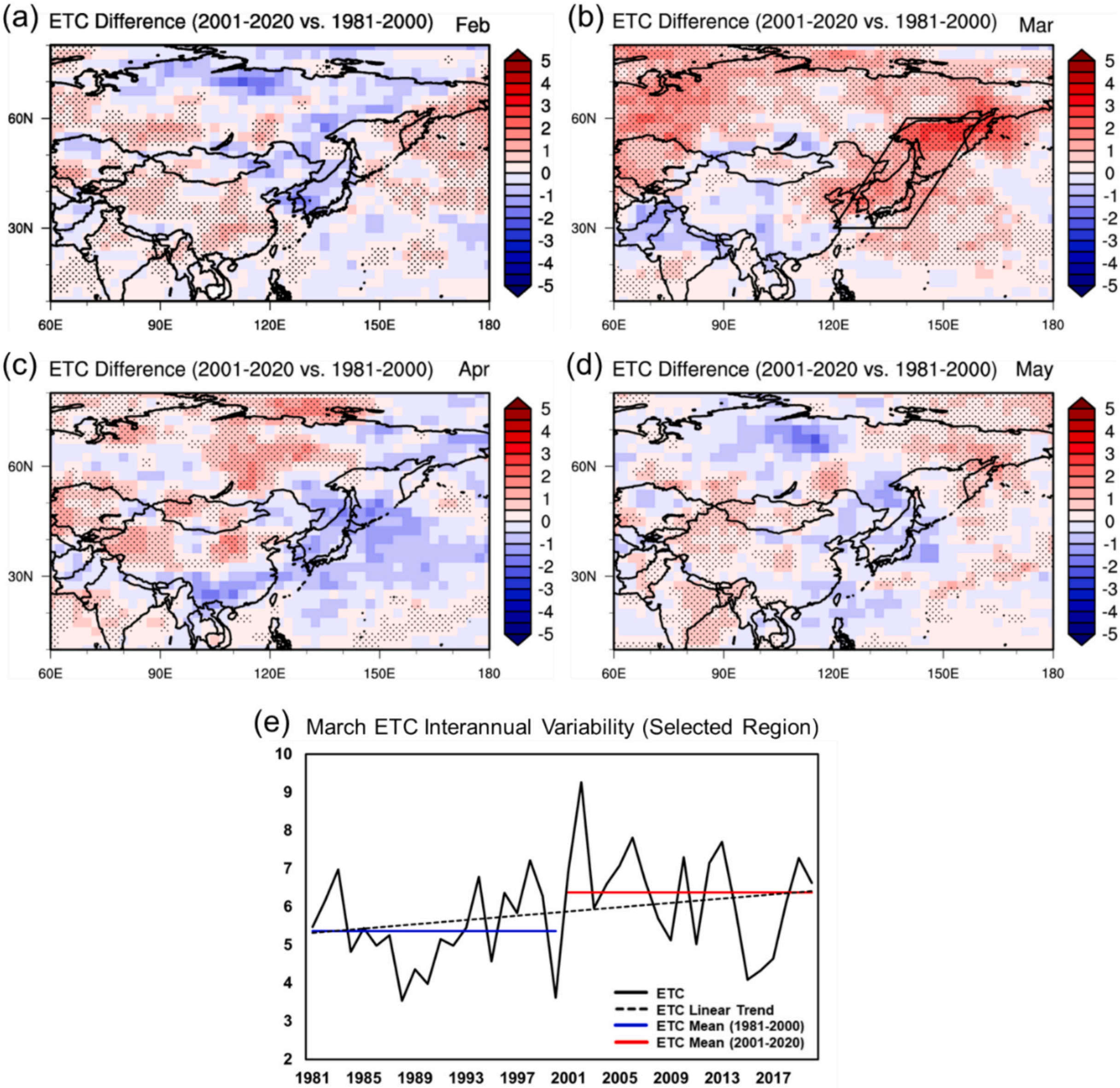

Fig. 1. Spatial differences in the locations of maximum extratropical cyclone (ETC) intensity between 2001 and 2020 and 1981–2000 for (a) February, (b) March, (c) April, and (d) May. Dotted areas indicate statistically significant changes at the 95% confidence level. The outlined region in (b) marks the area where ETC intensity shows the strongest response in March. Panel (e) presents the area-averaged time series of ETC intensity over this region, highlighting the long-term trend and the mean values for each period.

reduction in sea-ice extent in the Sea of Okhotsk.

Sea ice in the Sea of Okhotsk has decreased steadily, with monthly reductions (January–April) of approximately 5.5%, 5.5%, 5.0%, and 5.9% per decade, respectively, from 1981 to 2020. During the post-2000 period, the monthly mean sea-ice extent decreased by 10.5%, 7.1%, 9.3%, and 14.0% (January–April, respectively) relative to the pre-2000 period (Fig. S5). The increase in air temperature over the Sea of Okhotsk during the post-2000 period (Fig. 6g), attributable to reduced cold advection from the north and enhanced warm advection from the south (Fig. 6b, e, h), led to a decrease in sea ice, promoting the development or intensification of a regional low (Fig. 3b) and associated cyclonic circulation (Fig. 6f). Indeed, Kamae and Yokota (2025) recently showed that the southerly winds in this region are closely related to the reduction the sea ice in the Sea of Okhotsk. Accordingly, it is plausible that the decline in sea ice over the Sea of Okhotsk contributed to the westward extension of the Aleutian Low and the emergence of a western core. As shown in the 925-hPa wind fields (Fig. 6i), northerly winds exhibited little change from Sakhalin to the southern part of the Korean Peninsula. However, because temperatures increased over Northeast Asia, including Primorsky (Fig. 6g) during the post-2000 period, cold advection in regions directly influenced by cold northerly winds, such as those adjacent to the East Sea/Sea of Japan and the Sea of Okhotsk, would instead have decreased (Fig. 6b, e). Contrastingly, southeasterly winds strengthened markedly from the south of the Japanese archipelago toward the Kamchatka Peninsula (Fig. 6i), and the associated warm temperature advection (Fig. 6h) and moisture transport (not shown) appeared to be the primary mechanisms responsible for atmospheric warming in this region.

Consequently, the westward tilt of the geopotential with height over the area (Fig. 5) is more attributable to the lower tropospheric warm advection induced by the enhanced southwesterly flow along the Japanese Archipelago than to an increase in cold advection associated with strengthened northerlies. Indeed, as illustrated in Fig. 5, the increase in geopotential thickness resulting from low-level warming contributed to

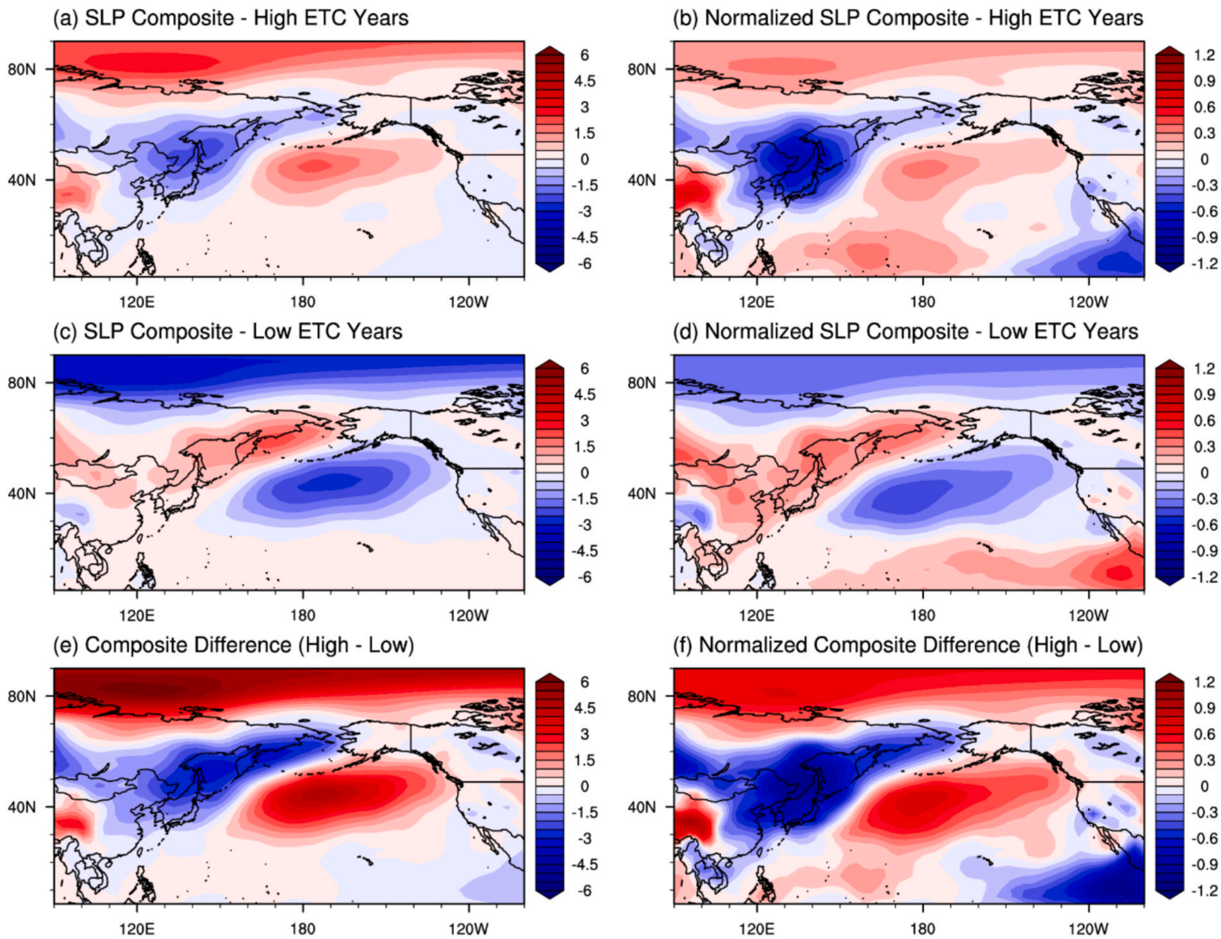

Fig. 2. Sea level pressure (SLP; unit: hPa) composites for (a) high ETC years and (c) low ETC years, defined based on years exceeding +0.43σ and below −0.43σ of the ETC time series. Panel (e) shows the composite difference (high minus low). Panels (b), (d), and (f) present the normalized fields, obtained by dividing the SLP anomalies at each grid point by their corresponding standard deviations.

the westward tilt of the geopotentials. The corresponding increase in atmospheric baroclinicity enhances eddy potential energy, which is closely linked to the intensified or increased development of mid-latitude cyclones in the region (Lorenz, 1955).

The zonally elongated warming from the Kuril Islands to the dateline (Fig. 6g) may be associated not only with the temperature advection discussed earlier but also with increases in SST between the two periods. Fig. 7 shows the SST and SST differences, revealing that SST increased across nearly all ocean basins, except for portions of the northeastern and equatorial eastern Pacific. Although the widespread SST increase is partly attributable to global warming, the spatial pattern of SST differences in the North Pacific closely resembles that of the negative phase of the PDO (e.g., Newman et al., 2016). This is consistent with the fact that after 1998, the PDO remained predominantly in its negative phase, except for two intervals (June 2014–August 2017 and November 2002–October 2003), whereas prior to 1998, it remained mostly in the positive phase, except during brief periods such as July 1988–July 1991 and July–December 1994. A prominent feature of the negative PDO phase is the presence of positive SST anomalies in the northwestern Pacific, and such SST increases can change surface heat fluxes, thereby affecting the middle and lower troposphere. Fig. 7f shows the differences in the net surface heat flux between the two periods, where positive (negative) values indicate that the ocean gained (lost) more heat through the surface compared to the pre-2000 period. Thus, as noted above, the SST and air temperature increased substantially from the eastern coast of Japan to the northwestern Pacific.

These SST changes, alongside the negative PDO phase, can be associated with ocean–atmosphere interactions as follows: Weakened northwesterly–westerly winds in the region (Fig. 6c, f) reduced cold advection (Fig. 6h), whereas enhanced warm air advection along the southern Japan Archipelago further increased lower-tropospheric temperatures. These conditions led to decreases in both the latent and sensible heat fluxes from the ocean to the atmosphere (Fig. S6). In other words, the combined effects of reduced cold advection, increased southerly flow that warmed the surface air, and weakened surface winds suppressed the upward heat fluxes, thereby contributing to the SST increase. Together with the SST increase associated with the negative PDO phase, these processes appear to have amplified SST warming in the region. Such coupled ocean–atmosphere feedback likely contributed to the concurrent increase in both surface air temperature and SST.

The increase in baroclinicity associated with the enhanced ETC-peak frequency in the region (Fig. 5) and the resulting increase in zonal eddy potential energy strengthened the upper tropospheric jet stream on the east side of the trough over the Bering Sea (Fig. S4 e, f), resulting in the jet shifting poleward. In addition, as the weakened Aleutian Low shifted toward the Kamchatka Peninsula, the meridional pressure gradient also reduced, causing the jet stream to weaken and its zonal extent to contract westward (Fig. 8a, b). Lee and Ahn (2017) suggested that the poleward shift of the jet in this region is, to some extent, related to the strengthening of the Hadley circulation, which intensifies the subtropical jet according to angular momentum conservation and to an increased meridional temperature gradient in the sinking branch associated with the expansion of the Hadley cell, and that such processes appear to be linked to global warming. Therefore, the poleward shift of the jet during

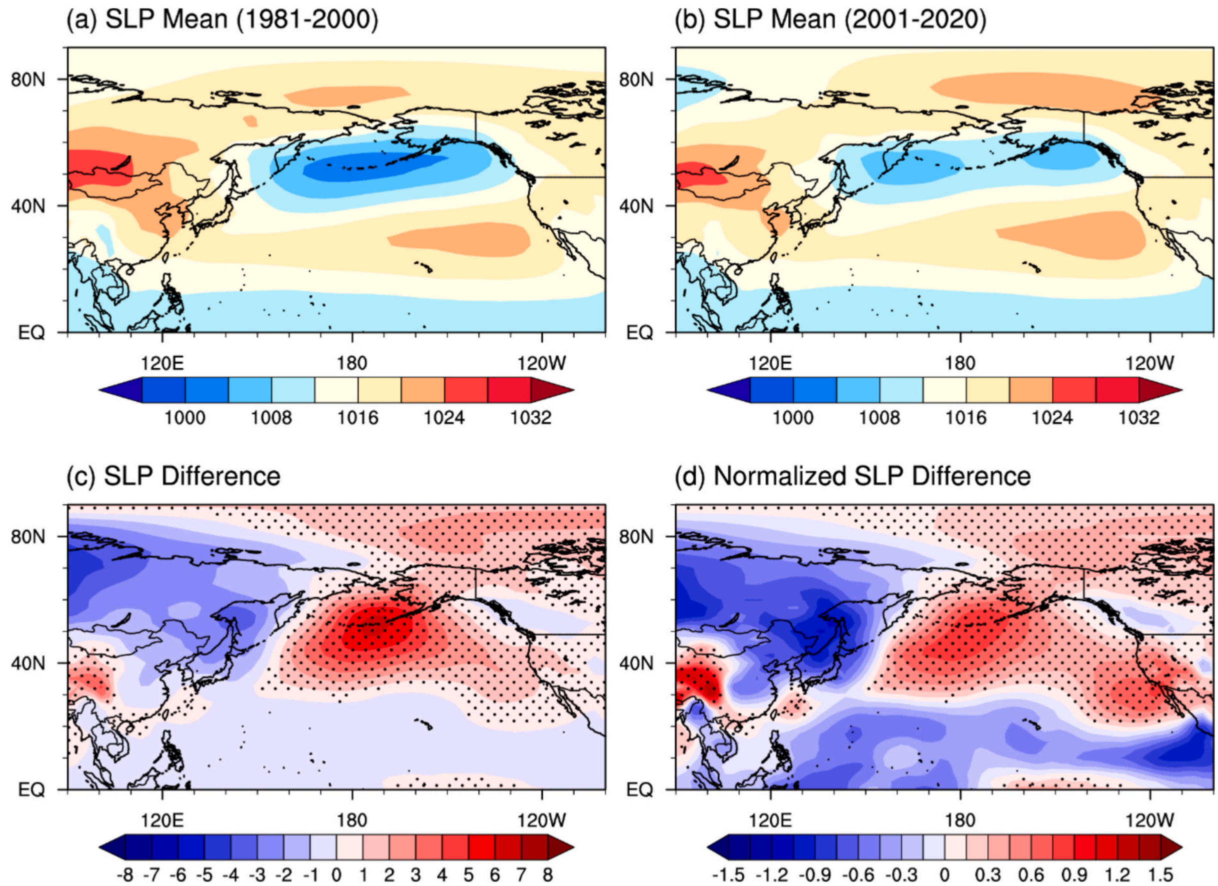

Fig. 3. (a) and (b) show the 20-year mean sea level pressure (SLP; unit: hPa) fields for the periods 1981–2000 and 2001–2020, respectively. Panel (c) presents the difference between the two periods (2001–2020 minus 1981–2000). Panel (d) displays the normalized SLP difference, obtained by dividing the anomalies at each grid point by their corresponding standard deviations. Dotted areas indicate statistically significant changes at the 95% confidence level.

early spring, together with changes in the Hadley circulation induced by global warming in this region, may also have contributed to the increase in the ETC activities. This will be discussed further in Section 4.

Fig. 9 shows the SLP distributions regressed onto ETC for the (a) pre-2000 and (b) post-2000 periods. As shown in Fig. 9a, a statistically significant SLP pattern associated with the ETC-peak frequency was not found around the marginal seas of the WNP during the pre-2000 period. Contrastingly, during the post-2000 period (Fig. 9b), negative SLP correlation with the ETC-peak frequency predominated over the area, whereas positive SLP correlations were observed from the central North Pacific to the Gulf of Alaska. This pattern closely resembles the differences between the post-2000 and pre-2000 periods shown in Fig. 3c and d. This indicates that, while changes in SLP over the region were absent or statistically insignificant in relation to ETC during the pre-2000, the pressure changes that emerged over and around the region during the post-2000 were significantly correlated with the ETC-peak frequency variations.

3.2. Analysis based on large-scale climate indices

In the previous section, we examined the changes in the climatological synoptic conditions responsible for the increase in ETC-peak frequency over the region during the post-2000 period. In this section, we aim to understand the fundamental drivers of enhanced ETC-peak frequency from a large-scale perspective by investigating the correlations between ETC-peaks and large-scale climate indices. As indicated in the earlier analyses, the major variables related to ETC-peaks exhibit substantial changes between the pre-2000 and post-2000 periods, and the correlations are examined separately for the two periods. Table 2 presents the simultaneous correlations between ETC-peak frequency and 16 large-scale indices.

As shown in Table 2a, no large-scale indices exhibited statistically significant correlations (at the 90% confidence level or higher) with ETC-peaks during the pre-2000 period. Contrastingly, during the post-2000 period (Table 2b), ETC-peaks showed statistically significant correlations with the WP index at the 99% level, and with the PDO index and Okhotsk sea ice coverage at the 95% confidence level. The correlation with the NAT index reached the 90% level, indicating a moderate relationship. A discussion on the NAT index is provided in Section 4. These results imply the presence of a climate regime shift around 2000 in terms of ETC activity. Analyzing the fundamental causes of such a regime shift is beyond the scope of this study. Subsequent discussions exclude indices that exhibit low statistical significance with respect to ETC-peaks.

3.2.1. Relationship between ETC-peak and WP pattern

Fig. 10a and c show the SLP composites for the years with a positive WP phase ($> +0.43$ STD) during the pre-2000 and post-2000 periods, respectively. Because the patterns associated with negative WP years are nearly the opposite of those associated with positive WP years, the discussion focuses on the positive WP phase. In the North Pacific, both periods exhibited a negative anomaly north of the Aleutian Islands and a zonally positive anomaly near 40°N, indicating that the overall spatial structure of the positive WP pattern for both periods was similar to some extent. During the pre-2000 period, however, the negative anomaly was centered over the Bering Sea, whereas the positive anomaly extended zonally from Primorye through the East Sea/Sea of Japan to the Gulf of Alaska. In contrast, during the post-2000 period, the core of the negative

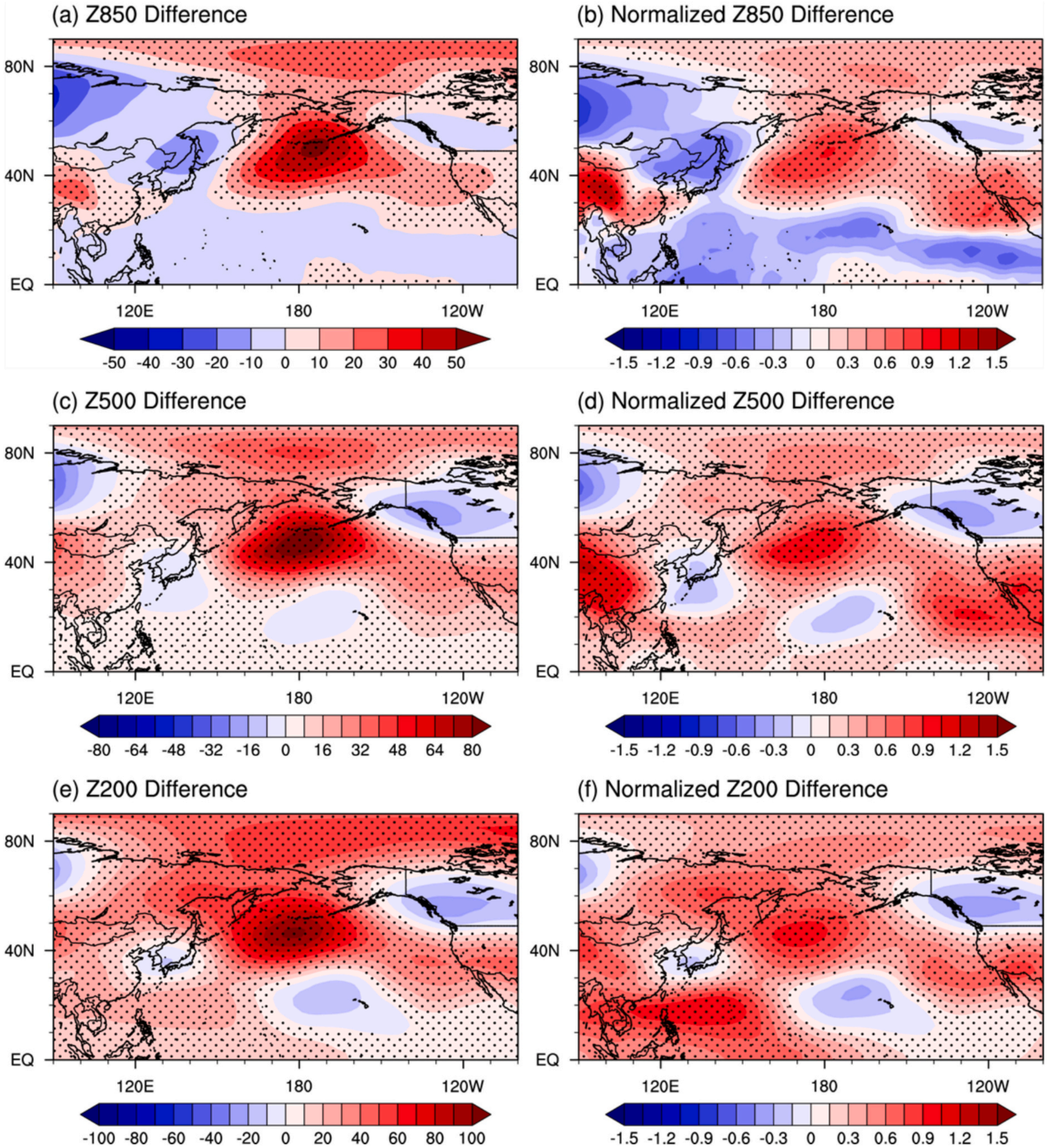

Fig. 4. Differences in geopotential height(unit: gpm) at (a) 850 hPa, (c) 500 hPa, and (e) 200 hPa between 2001 and 2020 and 1981–2000. Panels (b), (d), and (f) present the corresponding normalized fields, obtained by dividing the anomalies at each grid point by their standard deviations. Dotted areas indicate statistically significant changes at the 95% confidence level.

anomaly shifted toward the Kamchatka Peninsula, and negative anomalies appeared over the Korean Peninsula, Primorye, and the Sea of Okhotsk. The positive anomaly was centered near the dateline at 40°N and extended from the region south of Japan to the Gulf of Alaska. This suggests that during the pre-2000 period, the cyclonic activity was relatively weak over the region around the marginal seas of the western North Pacific and their vicinities during positive WP years, whereas in the post-2000 period, the cyclonic activity increased under positive WP conditions. The pattern of North Pacific SLP anomalies during positive WP years in the post-2000 period (Fig. 10c) resembles the SLP differences between the post-2000 and pre-2000 periods shown earlier in Fig. 3c, d. As discussed in the previous section, this structure provides conditions more conducive to cyclone development over the region. Moreover, the combination of negative SLP centered over the Kamchatka Peninsula and positive SLP south of the Aleutian Islands during positive WP phases forms an SLP structure that enhances the northward transport of warm, moist air from the Philippine Sea and the WNP toward the waters south of Japan along the Kuroshio Current.

Notably, during the pre-2000 period, both positive and negative WP phases exhibited positive SLP anomalies over the Sea of Okhotsk. In contrast during the post-2000 period, negative and positive SLP anomalies appeared over Sea of Okhotsk and the Kamchatka Peninsula for positive and negative WP years, respectively. Considering that negative (positive) SLP anomalies in the region generally indicate enhanced (suppressed) mid-latitude cyclone activity or more (less) favorable conditions for their development, ETC activity during the pre-2000 period was not statistically linked to the WP phase, whereas in the post-2000 period, cyclone activity became more enhanced during

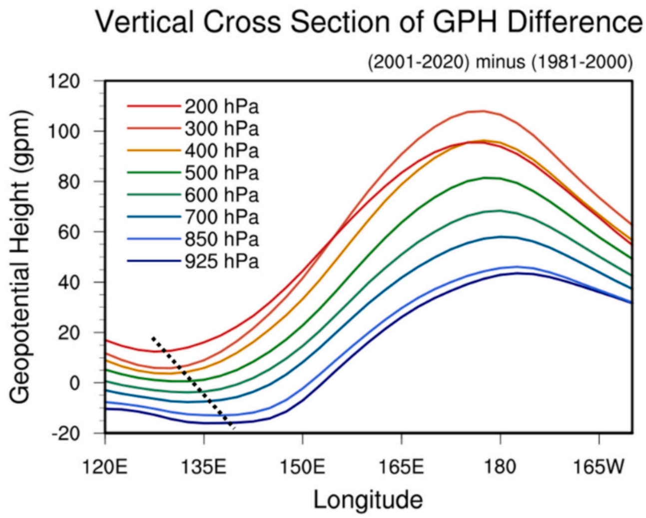

Fig. 5. Geopotential height (GPH) difference (unit: gpm) in a vertical cross section meridionally averaged over 40–50°N. The difference is calculated between the post-2000 period (2001–2020) and the pre-2000 period (1981–2000). Colored solid lines indicate representative pressure levels from 925 to 200 hPa.

positive WP years and weaker during negative WP years.

Accordingly, as shown in Table 2, the relationship between the ETC-peak frequency and WP was statistically insignificant during the pre-2000 period (r = 0.26), whereas a highly significant correlation emerged during the post-2000 period (r = 0.58). Among the various large-scale indices, the WP pattern exhibited the strongest correlation with the number of ETC-peaks during the post-2000 period, implying that the influence of WP on the region substantially increased from the year 2000. The significant change in the statistical relationship between ETC and the WP index around 2000 appears to be associated with the apparent negative SLP anomalies over the Kamchatka Peninsula in particular, under positive WP conditions. A more detailed discussion of the possible underlying causes is provided in Section 4 (Discussion).

3.2.2. *Relationship between ETC-peak and PDO*

During the post-2000 period, the PDO index exhibited the second-highest correlation with ETC activity, following the WP index. Fig. 11 presents the SLP composites for years in which the PDO exceeded +0.43 STD and fell below −0.43 STD during the pre-2000 and post-2000 periods. As shown in the figure, during the pre-2000 period, positive PDO phases were characterized by a broad negative anomaly centered over the Aleutian Islands in the North Pacific, accompanied by positive anomalies over the equatorial western Pacific, northeastern Asia, and Canada (Fig. 11a). During negative PDO phases, negative anomalies extended across North America, with a center over the Bering Sea,

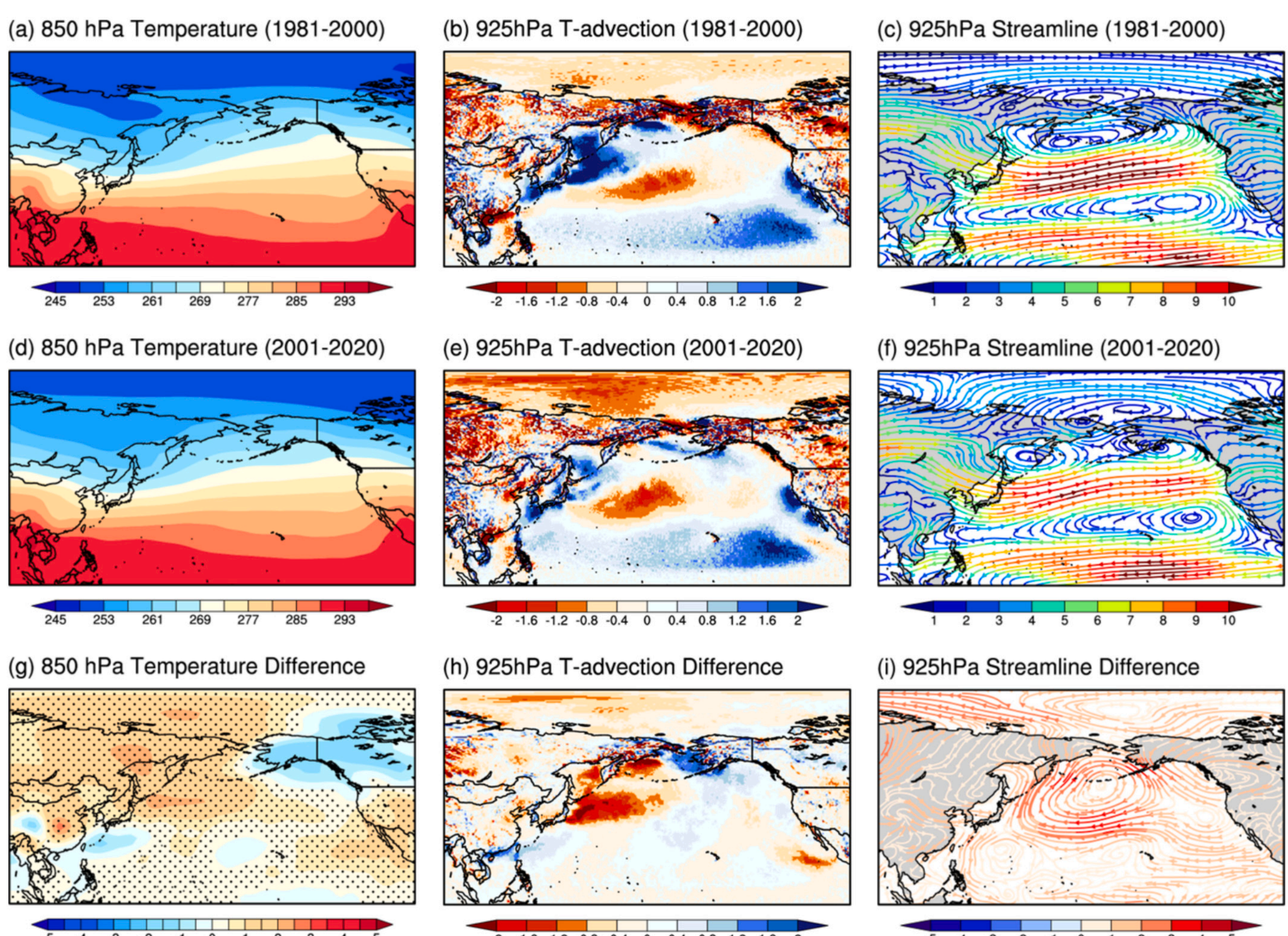

Fig. 6. Spatial patterns of (a, d) 850 hPa temperature (unit: K), (b, e) 925 hPa temperature advection (unit: K/day), and (c, f) 925 hPa streamlines for the climatological means of 1981–2000 and 2001–2020. Panels (g–i) show the changes between the two periods (2001–2020 minus 1981–2000), highlighting regions with statistically significant differences at the 95% confidence level.

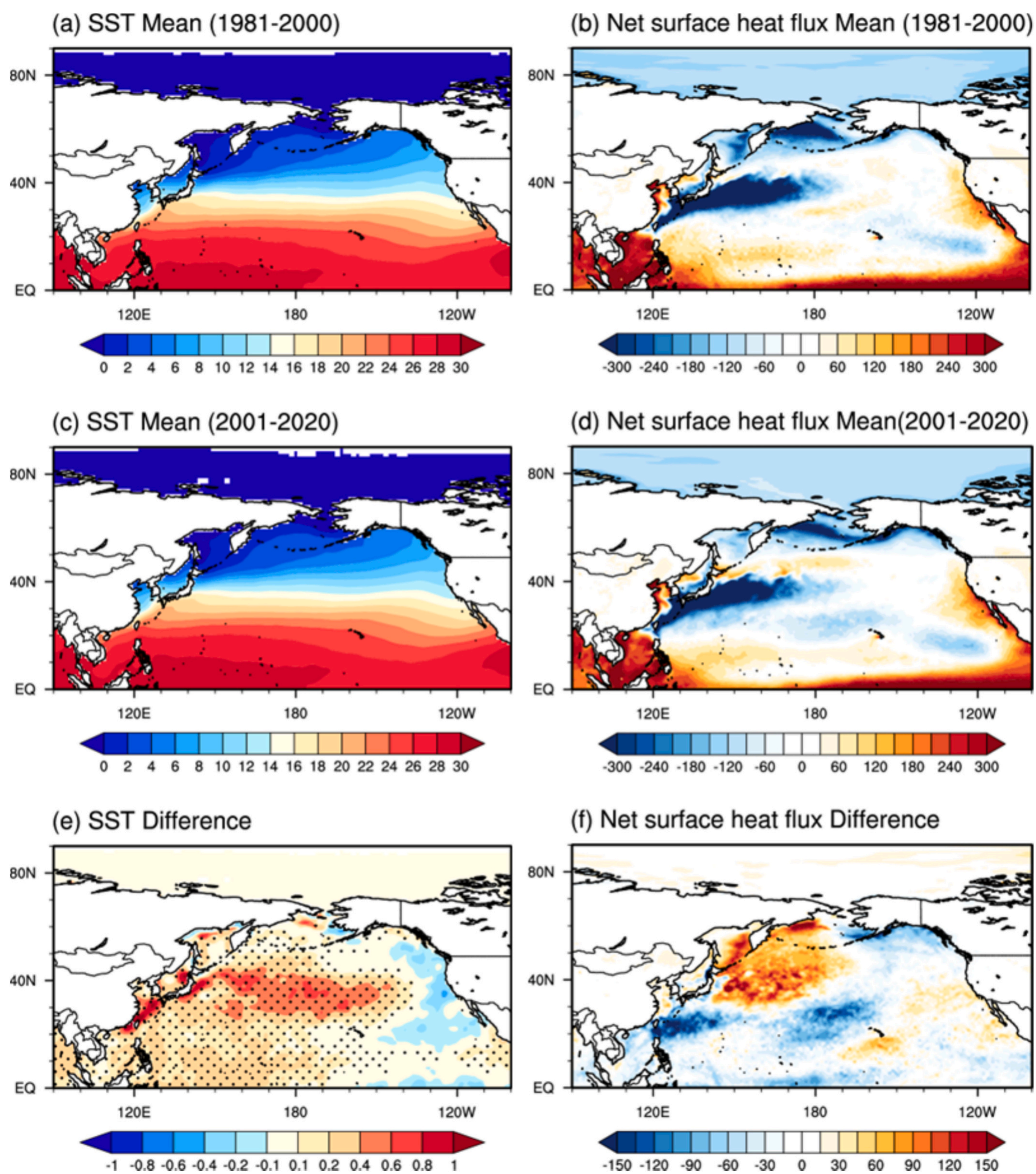

Fig. 7. Mean fields of (a, c) sea surface temperature (SST; unit: °C) and (b, d) net surface heat flux (unit: W/m^2) for the periods 1981–2000 and 2001–2020, respectively. Panels (e) and (f) show the differences between the two periods (2001–2020 minus 1981–2000). Dotted areas indicate statistically significant changes at the 95% confidence level.

whereas positive anomalies appeared over the Gulf of Alaska and formed an elongated zonal band across Primorye and the Japanese Archipelago. During the post-2000 period, positive PDO phases featured positive anomalies over the Bering Sea and the ETC-peak region, with negative anomalies over the Gulf of Alaska. In contrast, negative PDO phases exhibited a large-scale dipole pattern across the North Pacific, characterized by a west–east dipole pattern around 160°E, with a negative anomaly to the west and a positive anomaly to the east. Specifically, negative anomalies occurred over the western Sea of Okhotsk, Korea, Japan, and Primorye, whereas positive anomalies appeared broadly over

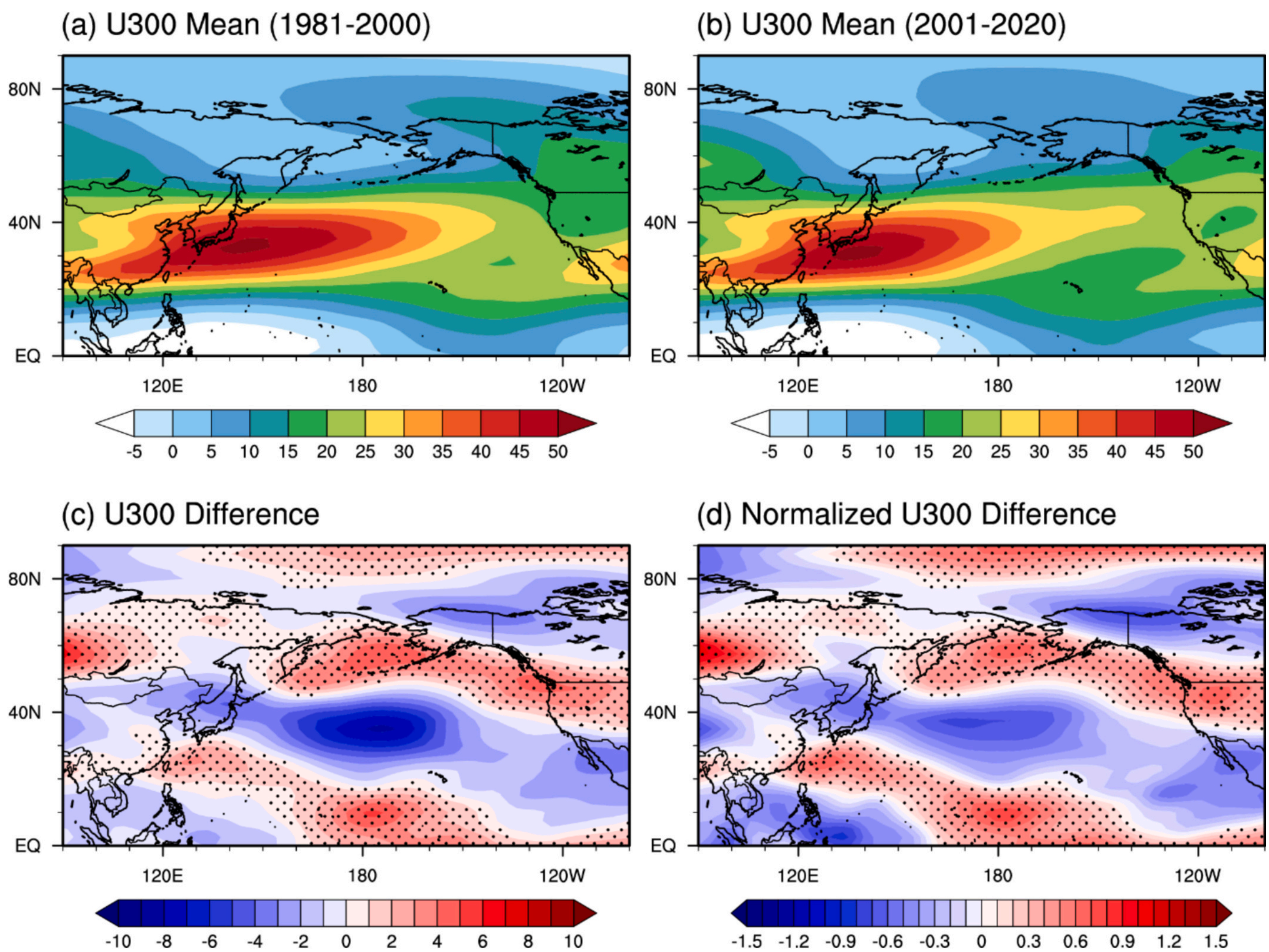

Fig. 8. Mean 300-hPa zonal wind (U300; unit: m/s) fields for (a) 1981–2000 and (b) 2001–2020. Panel (c) presents the difference between the two periods (2001–2020 minus 1981–2000), and (d) shows the corresponding normalized U300 difference, obtained by dividing the anomalies at each grid point by their standard deviations. Dotted areas indicate statistically significant changes at the 95% confidence level.

the Aleutian Islands, Gulf of Alaska, and Alaska.

In the pre-2000 period, positive SLP anomalies appeared over the ETC-peak region during both positive and negative PDO phases, whereas in the post-2000 period, positive and negative anomalies were distinctly associated with positive and negative PDO years, respectively. Therefore, the influence of the PDO on the ETC activity over the region was unclear during the pre-2000 and became more pronounced during the post-2000. Specifically, during the pre-2000 period, there was no statistically significant relationship between PDO and ETC-peak, whereas in the post-2000 period, years with a negative PDO were associated with enhanced cyclone activity, and years with a positive PDO corresponded to suppressed cyclone activity. Accordingly, as shown in Table 2, no statistically significant correlation between the ETC-peak frequency and PDO was observed during the pre-2000 ($r = -0.36$), whereas a significant correlation emerged during the post-2000 ($r = -0.48$). This indicates that, similar to WP, the effect of the PDO on the ETC activity in this region became evident after 2000.

Notably, the negative PDO pattern in the post-2000 period closely resembled the SLP difference between the post-2000 and the pre-2000 periods (Fig. 3c,d). Specifically, the negative differences were located over Korea, Japan, and Primorye, centered around Sakhalin, whereas the positive differences were broadly distributed over the Aleutian Islands, Gulf of Alaska, and Alaska. This indicates that a negative PDO pattern was dominant in the post-2000 period**.** In contrast, during the pre-2000 period, even in negative PDO years, positive SLP anomalies appeared over the region. This further suggests that the influence of the PDO on the ETC-peak activity was not apparent in the pre-2000 period. In other words, the post-2000 negative PDO phases provided conditions favorable for mid-latitude ETC activity over the region, whereas opposite conditions prevailed during the pre-2000 period. Consequently, during the post-2000 period, which was dominated by the negative PDO phase, the atmospheric environment over the ETC-peak area became more conducive to the development of low-pressure systems.

The composite and statistical analyses presented above and in Section 3.2.1 indicate that, while the overall influence of the PDO across the North Pacific remains broadly similar between the two periods, its impact on the region has undergone a substantial change to the extent that SLP anomalies exhibit opposite signs.

3.2.3. Combined influence of WP and PDO on ETC-peak

As discussed above, unlike the pre-2000 period, years characterized by either a positive WP or a negative PDO during the post-2000 period exhibited negative SLP anomalies over the region, creating a more favorable environment for ETC-peaks. Additionally, a positive SLP anomaly over the northwestern Pacific, where the Kuroshio Extension is located, established a pressure pattern that facilitated the intrusion of warm and moist air from the south into the region. This inflow enhances the baroclinicity over the region, thereby providing conditions more

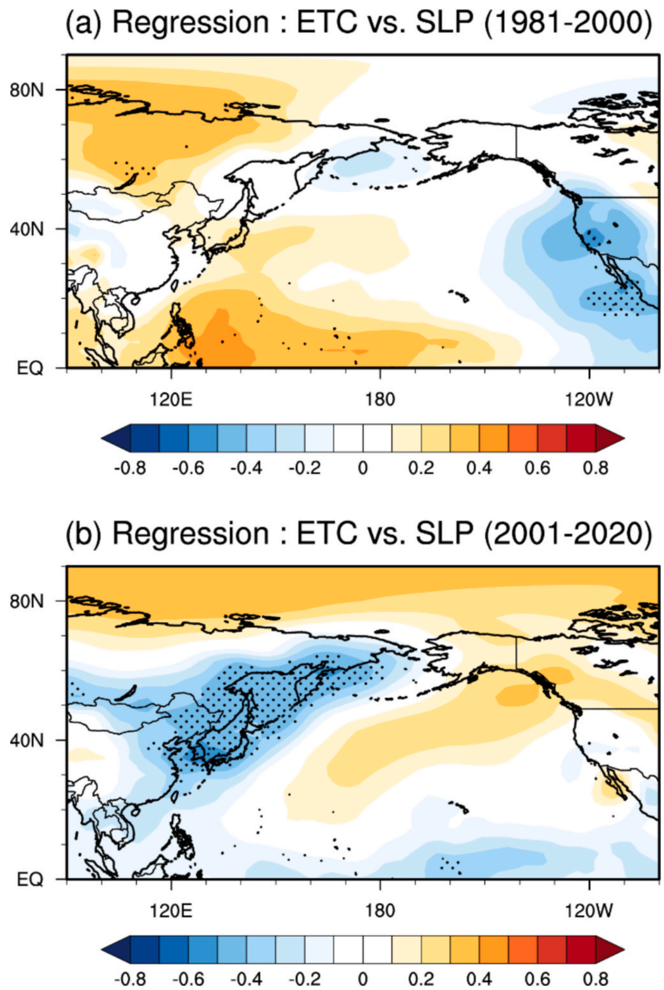

Fig. 9. Spatial regression patterns between the ETC time series at the maximum ETC activity region (Fig. 1e) and normalized sea level pressure (SLP) anomalies for the periods (a) 1981–2000 and (b) 2001–2020. Shaded and dotted regions represent statistically significant relationships at the 95% confidence level.

conducive to increased ETC development.

Fig. 12 illustrates March variations in the PDO and WP indices during the pre-2000 and post-2000 periods. The WP index exhibited no substantial trend over the 40-year period. The PDO index shows a pronounced decreasing trend, resulting in the majority of the post-2000 years being characterized by a negative PDO phase. Accordingly, the marked increase in the frequency of ETC-peak over the region during the post-2000 period compared with the pre-2000 period (Fig. 1) appears to be attributable to the predominance of the negative PDO phase. In contrast, the WP index did not serve as a direct driver of the post-2000 increase in ETC-peak, as the number of positive and negative WP years was comparable (19 and 21 years, respectively) over the entire 40-year period, and no clear trend is evident. The PDO index, however, exhibited a pronounced decreasing trend over the past four decades, with 14 years of a negative PDO phase during the post-2000 period. As discussed above, because PDO and ETC-peak are negatively correlated during the post-2000 period, the increased occurrence of negative PDO events after 2000 can be regarded as the primary driver of the enhanced ETC-peak over the region.

In addition, to quantitatively distinguish the respective contributions of interannual and interdecadal variability, we performed a multiple linear regression analysis for the post-2000 period. To assess the robustness of the results against long-term trends, the analysis was conducted using both original and detrended indices. After removing the linear trend, the statistical relationship became stronger: the model's total explanatory power (R^2) increased from 0.431 to 0.517, and the significance level of the PDO index improved from $p = 0.071$ to $p = 0.023$. Furthermore, the Variance Inflation Factor (VIF) for both indices was approximately 1.01, indicating negligible multicollinearity between the predictors. These results suggest that the PDO primarily contributes to the decadal background state, while the WP modulates interannual variability (Table S1).

Fig. 13 presents the time series of the WP and PDO indices overlapping with the ETC-peak frequency for the post-2000 period, during which both indices exhibited statistically significant correlations with ETC-peaks. As shown in the figure, years characterized by a negative PDO and a positive WP corresponded to relatively high ETC-peak frequencies, whereas years with a positive PDO and a negative WP exhibited relatively lower ETC-peak frequencies. Therefore, under the prevailing negative PDO conditions during the post-2000 period, the occurrence of positive WP phases further enhanced ETC activity.

4. Conclusions and discussion

4.1. Conclusions and summary

In this study, we examined the statistically significant increase in

Table 2
Correlation coefficients between the climate indices used in this study and the frequency of Extratropical Cyclones (ETCs) for the periods (a) 1981–2000 and (b) 2001–2020. Statistical significance is indicated by asterisks: * for the 90% confidence level ($p < 0.10$), ** for the 95% confidence level ($p < 0.05$), and *** for the 99% confidence level ($p < 0.01$).

(a) 1981–2000				(b) 2001–2020			
	ETC	WP	PDO		ETC	WP	PDO
WP	0.26			WP	0.58***		
PDO	0.36	−0.17		PDO	−0.48**	−0.1	
ENSO	0.32	0	0.43*	ENSO	−0.09	0.17	0.68***
IOD	0.04	0	−0.09	IOD	0.03	−0.07	−0.35
PJ	0.06	0.60***	−0.47**	PJ	0.23	0.65***	−0.06
EA/WR	0.11	0.2	−0.18	EA/WR	0.29	0.51**	−0.15
AO	−0.16	−0.27	−0.37	AO	−0.32	−0.31	0.1
EAWMSLP	−0.33	−0.13	−0.16	EAWMSLP	−0.11	−0.4	−0.18
EAWMU300	−0.14	−0.36	0.33	EAWMU300	−0.16	−0.44*	0.06
EAWMZ500	0.17	0.52**	−0.35	EAWMZ500	−0.13	0.26	0.18
EAJSI	−0.15	−0.37	0.37	EAJSI	0.02	−0.3	0.03
WPSH	0.33	0.26	0.38*	WPSH	−0.04	0.39*	0.52**
ISM	−0.32	−0.01	−0.31	ISM	0.01	−0.31	−0.47**
EASM	−0.2	0.24	−0.57***	EASM	0.11	0.23	−0.23
OK Sea Ice	−0.07	0.38*	−0.29	OK Sea Ice	0.46**	0.41	−0.22
NAT	0.27	0.19	0.40*	NAT	0.42*	0.12	−0.21

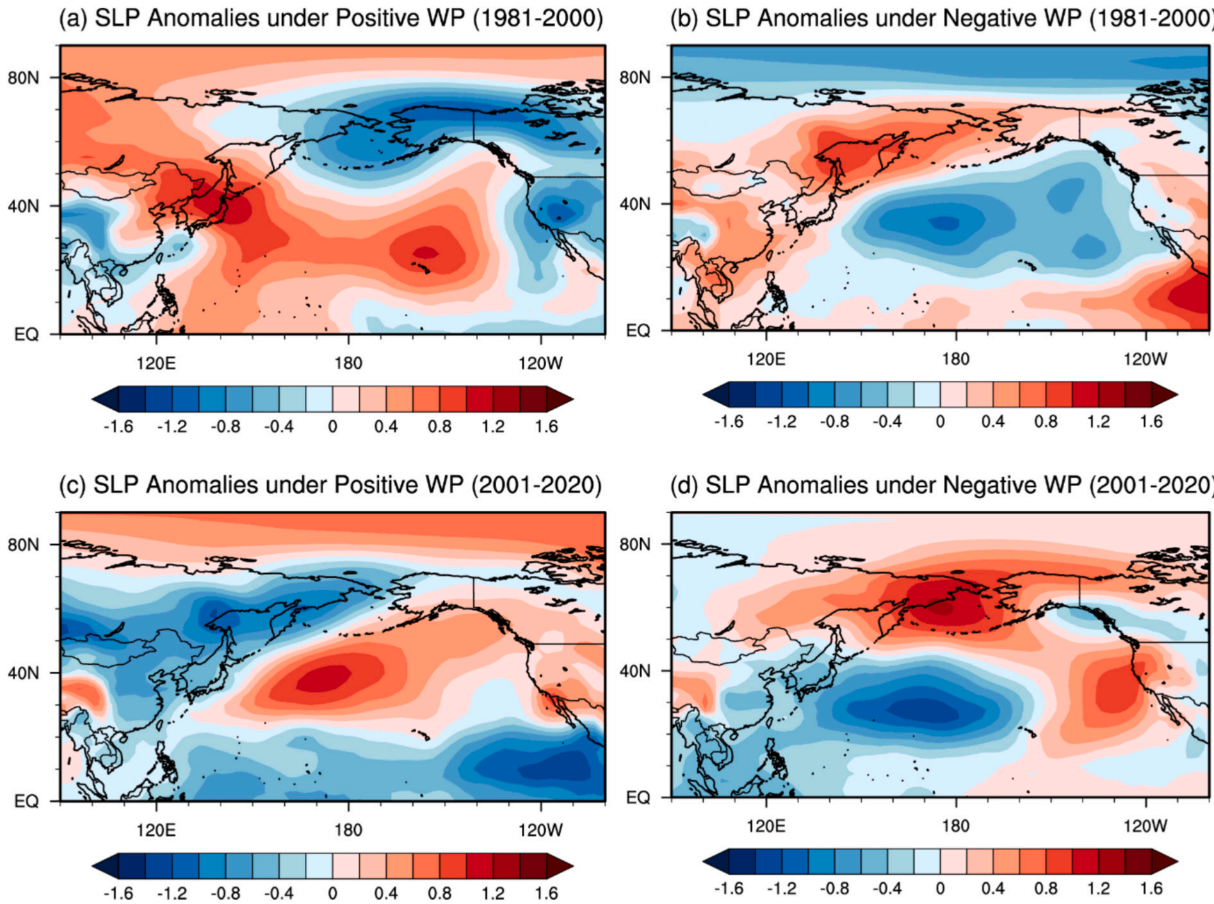

Fig. 10. Composite patterns of normalized sea level pressure (SLP) anomalies under (a, c) positive and (b, d) negative phases of the Western Pacific (WP) pattern, separated into the periods 1981–2000 and 2001–2020.

ETC-peak occurrences over the ETC-peak region during early spring after 2000 and analyzed the factors contributing to this change. For this purpose, we defined the pre-2000 and post-2000 periods to represent the two-decade periods before and after 2000, respectively.

A composite analysis comparing the pre- and post-2000 periods indicated that during the post-2000 period, a negative SLP anomaly was located over the ETC-peak area, spanning the Sea of Okhotsk, Russian Far East, Japan, and Korea, creating favorable conditions for enhanced cyclone development. Specifically, the increase in the negative SLP anomaly over the northwestern sector centered on the Sea of Okhotsk, together with the strengthening of positive SLP anomalies in the North Pacific south of the Aleutian Islands, led to an increased SLP gradient along the corridor from the southeastern coast of Japan to the Kamchatka Peninsula. This enhanced gradient facilitated the advection of warm and moist air from the southeast, thereby establishing an environment conducive to cyclone development. This climatological synoptic SLP distribution was not observed during the pre-2000 period. SLP distributions regressed onto ETC-peaks for the two periods further supported this pattern. That is, while no statistically significant relationship between SLP and the ETC-peak frequency in the region was evident during the pre-2000 period, in the post-2000 period, negative SLP correlations with the ETC-peak frequency appeared over northeastern Asia, including the Korean Peninsula, Sea of Okhotsk, and Kamchatka Peninsula, and positive SLP correlations extending from the central North Pacific to the Gulf of Alaska appeared.

Analysis of the vertical geopotential structure over the region indicates that, compared to the pre-2000 period, an anomalous negative trough centered on the Sea of Okhotsk extends upward and tilts westward, producing a baroclinic structure. The increase in baroclinicity is not primarily due to enhanced cold air advection from the northeast into the region, but rather to stronger warm air advection from the southeast, which increases the thickness of the warm air layer and causes the trough to tilt westward. Specifically, compared with the pre-2000, the post-2000 period was characterized by a weakened Aleutian Low and Siberian High, reducing the overall pressure gradient, while surface temperatures northwest of the region, including the Russian Far East, increased, weakening the cold air flow. Simultaneously, enhanced warming in the southeast, together with an anomalous low-west/high-east type pressure distribution, increased warm air advection. Consequently, the main contributor to the enhanced baroclinicity over the region was the increased advection of warm air from the southwest. This enhanced baroclinicity led to an increase in zonal eddy available potential energy, rendering the region more conducive to cyclone development during the post-2000 period.

Another possible contributor to the increased negative SLP anomalies over the ETC region during the post-2000 period is the regional warming and the associated reduction in Okhotsk Sea ice. The increased warm southerly wind and the decreased cold northerly wind anomalies enhance near-surface air temperature over the region and promote sea-ice melt in the Sea of Okhotsk. Decreased sea-ice, which is significantly correlated with the increased ETC activity, weakens the subsidence motion over the Sea of Okhotsk and induces anomalous lows. Thus, the reduced sea-ice cover as well as the positive temperature anomalies over the region contribute to the decrease in SLP, thereby forming conditions more favorable for the cyclone development in the region. Our results also suggest that while Okhotsk sea-ice reduction may physically favor the development of a cyclonic environment, its variability is largely modulated by or embedded within the larger-scale regime shift

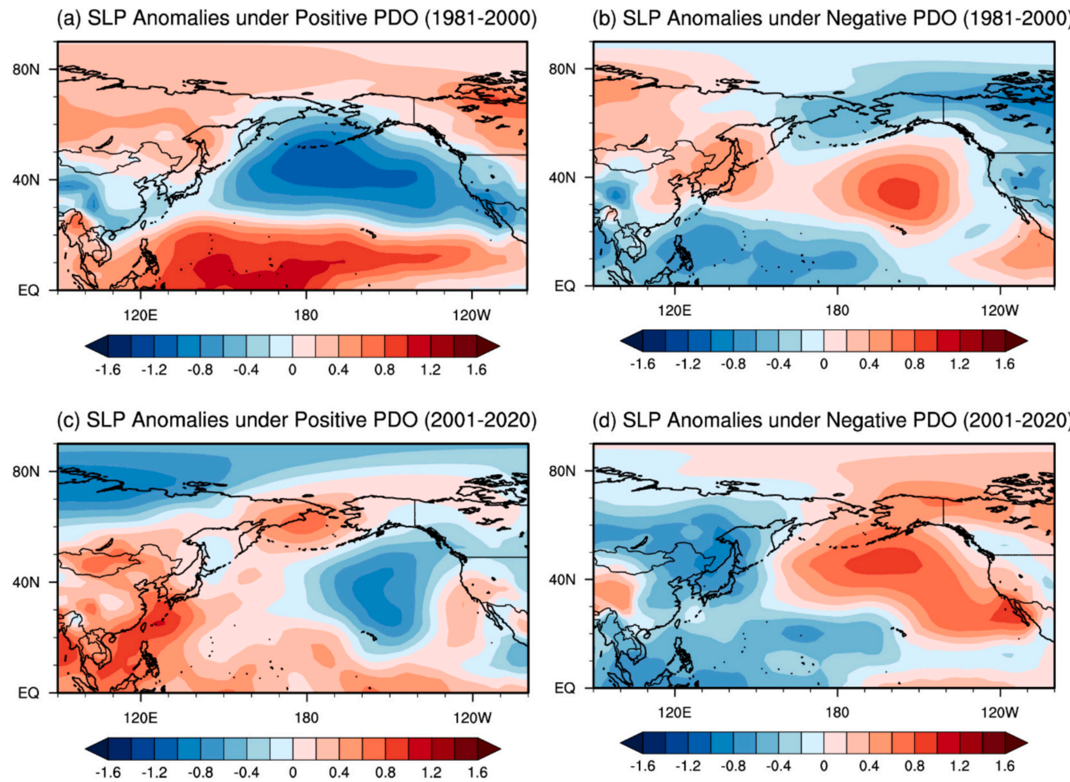

Fig. 11. Composite patterns of normalized sea level pressure (SLP) anomalies under (a, c) positive and (b, d) negative phases of the Pacific Decadal Oscillation (PDO) for the periods 1981–2000 and 2001–2020.

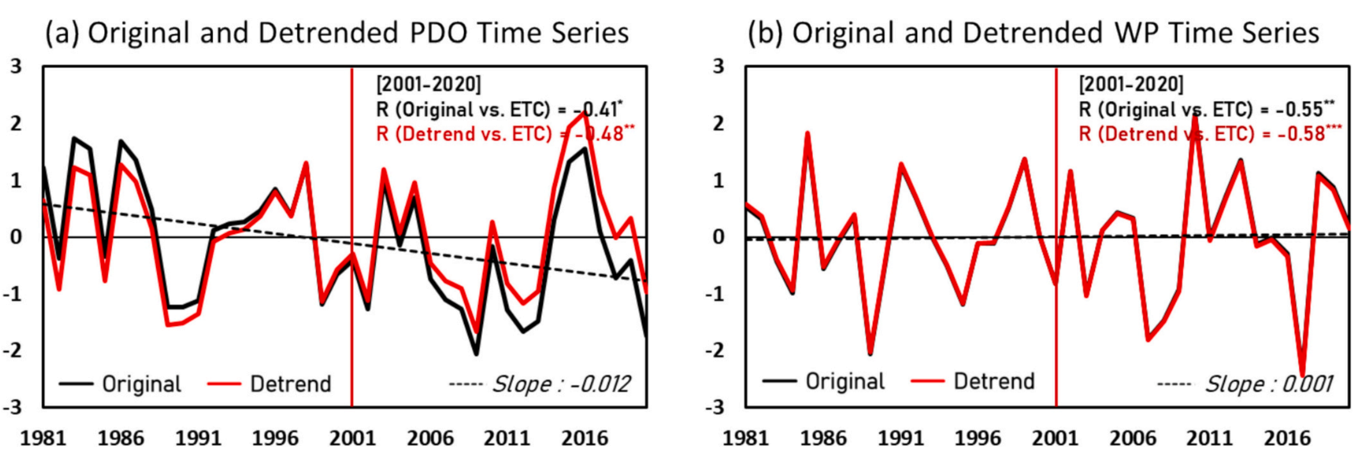

Fig. 12. Original (black) and detrended (red) time series of the (a) PDO and (b) WP indices from 1981 to 2020. The vertical red line marks the boundary between the two analysis periods (1981–2000 and 2001–2020). Correlation coefficients between each index and ETC intensity are shown for the recent period (2001–2020), based on both the original and detrended series. Slopes represent the linear trends of the original time series. Statistical significance is indicated by * ($p < 0.1$), ** ($p < 0.05$), and *** ($p < 0.01$). (For interpretation of the references to colour in this figure legend, the reader is referred to the web version of this article.)

(Table S2). Thus, it would be reasonable to conclude that the PDO plays a primary role in establishing the decadal background state, while local sea ice changes may act as a reinforcing factor.

To understand the increase in ETC-peak occurrence in terms of large-scale climate variability, we examined the correlations between various large-scale climate indices and ETC-peak frequency. During the pre-2000 period, none of the indices exhibited statistically significant relationships with ETCs. In contrast, during the post-2000 period, both the WP and PDO indices showed statistically significant correlations with ETC-peaks. This is likely because the spatial patterns of the WP and PDO over the region underwent substantial changes relative to the pre-2000 period. Specifically, in the post-2000 period, positive (negative) WP phases were associated with negative (positive) SLP anomalies over the region, providing conditions more (less) favorable for ETC-peak occurrence. Similarly, negative and positive PDO phases produced pressure distributions over the region resembling those associated with the positive and negative WP phases, respectively. In contrast, during the pre-2000 period, positive SLP anomalies were observed over the region regardless of whether the WP phase was positive or negative. A similar result was found for the PDO: both positive and negative PDO phases were associated with positive SLP anomalies over the region. This suggests that, prior to 2000, variations in the PDO and WP phases were not strongly linked to SLP variability in this region. This interpretation is consistent with the statistical results indicating that PDO/WP variations

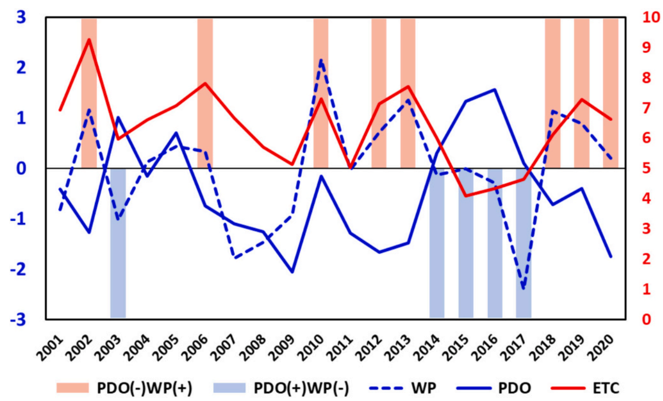

Fig. 13. Time series of the PDO (solid blue), WP (dashed blue), and ETC (red) indices during 2001–2020. Shaded bars highlight years when PDO and WP were in opposite phases, with red shading indicating PDO negative and WP positive, and blue shading indicating PDO positive and WP negative. The ETC index values correspond to the right vertical axis. (For interpretation of the references to colour in this figure legend, the reader is referred to the web version of this article.)

were not significantly associated with ETC activity during the pre-2000 period.

The statistically significant post-2000 correlations of ETC activity with WP and PDO can also be understood as a consequence of background-state changes associated with the PDO regime shift. The transition from a positive to a negative PDO regime altered the large-scale atmospheric and oceanic mean state, such that the Aleutian Low weakened and shifted westward (Newman et al., 2016), and meridional SST gradients over the WNP were enhanced, resulting in a westward-displaced jet stream. These changes may have modified Rossby wave propagation pathways, enhancing regional baroclinicity and eddy growth efficiency, and may have promoted a more constructive alignment between the background circulation and WP-related anomalies. As a result, WP and PDO signals may have projected more effectively onto extratropical cyclone variability over the region after 2000, whereas before 2000 their influence may have been masked or diluted by the prevailing background flow.

While the WP index exhibited little long-term trend, with roughly equal numbers of positive and negative years throughout the entire period, the PDO index showed a clear decreasing trend, with most post-2000 years occurring in its negative phase. Therefore, from the perspective of large-scale climate patterns, our results suggest that although the WP appears to have influenced interannual variability of ETC activity over the region, the PDO-driven background-state changes likely played a substantial role in the observed increase in ETC-Peak occurrence during the post-2000 period.

4.2. Discussion

In the previous sections, we showed that the WP index–ETC and PDO index–ETC linkages were not statistically significant before 2000, but became significant after 2000. We also demonstrated that ETC activity over the region decreased during the pre-2000 period and increased during the post-2000 period, along with associated climatological synoptic changes. However, the mechanisms underlying the post-2000 regime shift remain unclear, particularly why the springtime WP/PDO–ETC relationship became statistically significant only after 2000 and why regional ETC activity exhibits opposite tendencies between the two periods from a large-scale dynamical perspective.

To address these questions, it is necessary to first examine differences in the background state between the pre- and post-2000 periods. The pre-2000 period is characterized by a positive PDO regime, whereas the post-2000 period corresponds to a negative PDO regime (Fig. 12) (Newman et al., 2016). During the positive PDO phase, the Aleutian Low was intensified (Fig. 3a), the subtropical-to-midlatitude SST gradient was enhanced (Fig. 7a, e), and the Pacific jet was strong and zonally elongated (Fig. 8a). In contrast, during the negative PDO phase after 2000, the Aleutian Low weakened and shifted westward (Fig. 3b), while warmer SSTs in the WNP strengthened the meridional SST gradient near the ETC-peak region (Fig. 7c, e), resulting in a westward-displaced jet core (Fig. 8b). These changes in the background atmospheric–oceanic state likely modified the baroclinicity over the WNP (Fig. 5), altered eddy growth conditions, and shifted Rossby wave propagation pathways.

The appearance of the correlation of ETC activity with the WP index and PDO index after 2000 can be interpreted as being associated with by three primary dynamical mechanisms. First, enhanced baroclinicity over the region during the post-2000 period increased cyclone growth efficiency. Warming of SST and near-surface air temperature in the WNP under the negative PDO background strengthened lower-tropospheric thermal contrasts, thereby enhancing baroclinic instability. Consequently, this suggests that WP/PDO anomalies after 2000 projected onto a dynamically favorable growth environment. In contrast, during the pre-2000 period, even when WP anomalies occurred, the weaker baroclinic structure limited their amplification and reduced their impact on ETC variability.

Second, consistent with the decadal shift of the North Pacific jet and Aleutian Low (Linkin and Nigam, 2008), it is plausible that changes in the background flow may have altered the Rossby wave propagation pathway (Hoskins and Ambrizzi, 1993). That is, before 2000, the zonally elongated Pacific jet directed wave activity flux eastward toward North America, placing the ETC-peak region partly outside the primary waveguide. Moreover, strong background variability associated with the intensified Aleutian Low likely reduced statistical detectability, partially masking or redirecting WP/PDO teleconnection signals. After 2000, however, the westward shift of the jet core and enhanced meridional gradients over the WNP increased local baroclinicity and dynamically aligned the region with the stationary wave pattern. As a result, WP/PDO teleconnection signals may have exerted a stronger influence on the ETC development region.

Third, the mechanism may be interpreted in terms of destructive interference versus constructive alignment between the background circulation and WP-related anomalies. Prior to 2000, the positive PDO background circulation likely interfered destructively with WP-related anomalies, while strong Aleutian Low variability dominated North Pacific sea level pressure variance. This may have led to a statistical dilution of WP signals and a weak projection onto ETC variability. After 2000, the negative PDO background circulation may have become more structurally aligned with the spatial pattern of the WP, producing constructive interference. This alignment may have allowed ETC variability to increase coherently with the WP and PDO phases, thereby suggesting the background-state dependence of the teleconnection (Fig. S7).

To substantiate these interpretations, further investigation is needed to robustly quantify these underlying mechanisms and evaluate their relative contributions using additional diagnostics, such as wave activity flux, refractive index diagnostics, and baroclinic growth rate analyses.

While the PDO plays a primary role as discussed above, recent global warming may also contribute to the observed increase in ETC-peaks. Global warming induces changes in the global atmospheric pressure system, thereby altering the atmospheric general circulation. The recent increase in ETC-peaks may also be linked to such changes. However, the dataset used in this study spans only 40 years, which is insufficient to fully disentangle the effects of global warming and decadal-to-multidecadal climate oscillations on ETC activity. Thus, while the direct cause of the increased ETC-peaks in the post-2000 appears to be the change in the spatial pattern of the PDO during this period, it is also possible that warming-induced changes in the pressure field directly enhanced ETC activity over the region and that global warming influenced the PDO pattern itself. Consequently, future research should aim to assess the independent impacts of global warming and long-term climate variability, such as the PDO, on ETC activity in the region. Additionally, as demonstrated in this study, the northward shift of the jet stream in this region can be attributed to the strengthening of mid-latitude cyclones associated with variations in the PDO pattern over the North Pacific. However, as noted in Section 3.1.2, this shift may also be linked to changes in the Hadley circulation driven by global warming (e.g., Kim and Ahn, 2024). Disentangling the relative contributions of PDO variability and anthropogenic warming requires longer observational records that will enable such analyses in future research.

Notably, the transitions of the PDO and AMO to their negative and positive phases, respectively, occurred almost simultaneously around 2000 (Hu et al., 2011). If the phase transitions of the PDO and AMO occurred independently at different times, it would have been comparatively easier to isolate and diagnose the atmospheric pressure and circulation responses associated with each oscillation. However, the near-synchronous transitions of the PDO and AMO, together with ongoing global warming, make it challenging to disentangle the independent atmospheric responses to each mode of variability. Future studies should investigate the response of the earth system to such climate variabilities using numerical models, such as Coupled General Circulation Models.

Although the correlation between ETCs and the NAT pattern is not statistically significant at the 95% confidence level and was therefore not considered in the present analysis, it is noteworthy that the NAT exhibits a statistically significant relationship at the 90% confidence level with ETCs during the post-2000 period, whereas it was not significant in the pre-2000 period, similar to the PDO and WP. Previous numerical modeling studies suggest that sea-ice melting in the Sea of Okhotsk induces a negative 500 hPa anomaly, which in turn generates a positive NAT phase (+ − +) through a Rossby wave response (e.g., Screen, 2013; Wu et al., 2013). Although a debate over whether such localized forcing can produce a large-scale atmospheric response remains, the results from the model experiments highlight the need for further investigation in future studies.

CRediT authorship contribution statement

Yeomin Jeong: Writing – original draft, Visualization, Validation, Methodology, Investigation, Formal analysis, Data curation, Conceptualization. **Jong-Min Kim:** Formal analysis, Data curation. **Sera Jo:** Validation, Methodology. **Eung-Sup Kim:** Methodology, Investigation. **So-Hee Kim:** Software, Methodology. **Cheol-Hee Kim:** Writing – review & editing, Funding acquisition. **Joong-Bae Ahn:** Writing – review & editing, Validation, Supervision, Methodology, Conceptualization. **Hyo-Jung Lee:** Writing – review & editing, Supervision, Project administration, Conceptualization.

Declaration of competing interest

The authors declare that they have no known competing financial interests or personal relationships that could have appeared to influence the work.

Acknowledgement

This study was supported by the Cooperative Research Program for Agriculture Science and Technology Development (RS-2024-00400632), Rural Development Administration, Republic of Korea, and by the Basic Science Research Program through the National Research Foundation of Korea (NRF), funded by the Ministry of Education (RS-2020-NR049592, RS-2023-00247459).

Appendix A. Supplementary data

Supplementary data to this article can be found online at https://doi.org/10.1016/j.atmosres.2026.109001.

Data availability

The datasets analyzed in this study are publicly available from the respective data repositories cited in the manuscript.

References

Bader, J., Mesquita, M.D.S., Hodges, K.I., Keenlyside, N., Østerhus, S., Miles, M., 2011. A review on northern hemisphere sea-ice, storminess and the North Atlantic oscillation: Observations and projected changes. Atmos. Res. 101 (4), 809–834. https://doi.org/10.1016/j.atmosres.2011.04.007.

Barnston, A.G., Livezey, R.E., 1987. Classification, seasonality and persistence of low-frequency atmospheric circulation patterns. Mon. Weather Rev. 115 (6), 1083–1126. https://doi.org/10.1175/1520-0493(1987)115<1083:CSAPOL>2.0.CO;2.

Budikova, D., 2009. Role of Arctic sea ice in global atmospheric circulation: a review. Glob. Planet. Chang. 68 (3), 149–163. https://doi.org/10.1016/j.gloplacha.2009.04.001.

Chun, Y.S., Kim, J., Choi, J.C., Boo, K.-O., Oh, S.-N., Lee, M., 2001. Characteristic number size distribution of aerosol during Asian dust period in Korea. Atmos. Environ. 35, 2715–2721.

Czaja, A., Frankignoul, C., 2002. Observed impact of the North Atlantic oscillation on the North Atlantic Ocean surface. J. Clim. 15 (7), 684–696.

Emanuel, K., 2005. Increasing destructiveness of tropical cyclones over the past 30 years. Nature 436, 686–688.

Enfield, D.B., Cid-Serrano, L., 2010. Secular and multidecadal warmings in the North Atlantic and their relationships with tropical cyclone activity. Int. J. Climatol. 30 (2), 187–202. https://doi.org/10.1002/joc.1881.

Fu, S., Sun, J., Sun, J., 2014. Accelerating two-stage explosive development of an extratropical cyclone over the northwestern pacific ocean: a piecewise potential vorticity diagnosis. Tellus A 66 (1), 23210. https://doi.org/10.3402/tellusa.v66.23210.

Gao, J., Zhang, R.H., Zhi, H., 2025. Weakening of bomb cyclones over the north pacific in the early 21st century. Adv. Atmos. Sci. 42 (9), 1850–1862. https://doi.org/10.1007/s00376-025-4453-2.

Gao, X., Lu, P., Zhang, S., Hu, Y., Fu, G., Sun, X., Zhang, Q., 2022. A comparative study on initial developments between explosive and nonexplosive cyclones off the east asian coast in winter. Front. Earth Sci. 10, 968736. https://doi.org/10.3389/feart.2022.968736.

Hersbach, H., Bell, B., Berrisford, P., Hirahara, S., Horányi, A., Muñoz-Sabater, J., Nicolas, J., Peubey, C., Radu, R., Schepers, D., Simmons, A., Soci, C., Abdalla, S., Abellan, X., Balsamo, G., Bechtold, P., Biavati, G., Bidlot, J., Bonavita, M., De Chiara, G., Dahlgren, P., Dee, D., Diamantakis, M., Dragani, R., Flemming, J., Forbes, R., Fuentes, M., Geer, A., Haimberger, L., Healy, S., Hogan, R.J., Hólm, E., Janisková, M., Keeley, S., Laloyaux, P., Lopez, P., Lupu, C., Radnoti, G., de Rosnay, P., Rozum, I., Vamborg, F., Villaume, S., Thépaut, J.N., 2020. The ERA5 global reanalysis. Q. J. R. Meteorol. Soc. 146 (730), 1999–2049. https://doi.org/10.1002/qj.3803.

Hodges, K.I., 1994. A general-method for tracking analysis and its application to meteorological data. Mon. Weather Rev. 122 (11), 2573–2586. https://doi.org/10.1175/1520-0493(1994)122<2573:AGMFTA>2.0.CO;2.

Hodges, K.I., 1995. Feature tracking on the unit sphere. Mon. Weather Rev. 123 (12), 3458–3465. https://doi.org/10.1175/1520-0493(1995)123<3458:FTOTUS>2.0.CO;2.

Hodges, K.I., 1999. Adaptive constraints for feature tracking. Mon. Weather Rev. 127 (6), 1362–1373. https://doi.org/10.1175/1520-0493(1999)127<1362:ACFFT>2.0.CO;2.

Honda, M., Yamazaki, K., Tachibana, Y., Takeuchi, K., 1996. Influence of Okhotsk sea-ice extent on atmospheric circulation. Geophys. Res. Lett. 23 (24), 3595–3598. https://doi.org/10.1029/96GL03474.

Honda, M., Yamazaki, K., Nakamura, H., Takeuchi, K., 1999. Dynamic and thermodynamic characteristics of atmospheric response to anomalous sea-ice extent in the sea of Okhotsk. J. Clim. 12 (12), 3347–3358. https://doi.org/10.1175/1520-0442(1999)012<3347:DATCOA>2.0.CO;2.

Hong, J.-Y., Ahn, J.-B., 2015. Changes of early summer precipitation in the Korean peninsula and nearby regions based on RCP simulations. J. Clim. 28 (9), 3557–3578. https://doi.org/10.1175/JCLI-D-14-00504.1.

Hoskins, B.J., Ambrizzi, T., 1993. Rossby wave propagation on a realistic longitudinally varying flow. J. Atmos. Sci. 50 (12), 1661–1671. https://doi.org/10.1175/1520-0469(1993)050<1661:RWPOAR>2.0.CO;2.

Hoskins, B.J., Hodges, K.I., 2002. New perspectives on the northern hemisphere winter storm tracks. J. Atmos. Sci. 59 (6), 1041–1061. https://doi.org/10.1175/1520-0469(2002)059<1041:NPOTNH>2.0.CO;2.

Hsu, P.-C., Hsu, H.-H., Hong, H.-J., et al., 2025. Subtropical warming enhances north Pacific midlatitude winter storm track activity in recent decades. Npj Clim. Atmos. Sci. 8, 235. https://doi.org/10.1038/s41612-025-01108-7.

Hu, Z.-Z., McPhaden, M.J., Lee, S.-K., 2011. Historical and future patterns of the Atlantic multidecadal oscillation and their implications. J. Clim. 24 (6), 1404–1422. https://doi.org/10.1175/2010JCLI3861.1.

Jhun, J.G., Lee, E.Y., 2004. A new index for the east Asian winter monsoon and its relationship with the north pacific oscillation. J. Meteorol. Soc. Jpn. Ser. II 82 (2), 651–664.

Kamae, Y., Yokota, M., 2025. Southerly winds and rapid sea ice reductions along the sea of Okhotsk coast of Hokkaido. Meteorog. Atmos. Phys. 137, 4. https://doi.org/10.1007/s00703-024-01052-w.

Kamae, Y., Ueda, H., Inoue, T., Mitsudera, H., 2023. Atmospheric circulations associated with sea-ice reduction events in the Okhotsk sea. J. Meteorol. Soc. Jpn. 101 (2), 125–137.

Kanamitsu, T., Ebisuzaki, W., Woollen, J., Yang, S.-K., Hnilo, J.J., Fiorino, M., Kistler, M. G., 2002. The NCEP–NCAR reanalysis 2 project. Bull. Am. Meteorol. Soc. 83 (11), 1631–1643.

Kim, S.-H., Ahn, J.-B., 2024. Tropical cyclone landfalls in the northwest pacific under global warming. Int. J. Climatol. 44 (14), 4942–4962. https://doi.org/10.1002/joc.8616.

Kosaka, Y., Nakamura, H., 2010. Structure and dynamics of the Pacific-Japan pattern. Q. J. R. Meteorol. Soc. 136 (649), 1017–1033.

Kuwano-Yoshida, A., Asuma, Y., 2008. Numerical study of explosively developing extratropical cyclones in the northwestern pacific region. Mon. Weather Rev. 136 (2), 712–740. https://doi.org/10.1175/2007MWR2111.1.

Lau, K.-M., Li, M.-T., 1984. The monsoon of east Asia and its global associations — a survey. Bull. Am. Meteorol. Soc. 65 (2), 114–125.

Lee, J., Son, S.-W., Cho, H.-O., Kim, J., Cha, D.-H., Gyakum, J.R., Chen, D., 2020. Extratropical cyclones over east Asia: climatology, seasonal cycle, and long-term trend. Clim. Dyn. 54 (1–2), 1131–1144. https://doi.org/10.1007/s00382-019-05048-w.

Lee, J.-W., Ahn, J.-B., 2017. Future changes in the northern hemisphere summer subtropical jet in CMIP5 models. Theor. Appl. Climatol. 127 (3–4), 545–558. https://doi.org/10.1007/s00704-015-1647-y.

Linkin, M.E., Nigam, S., 2008. The North Pacific Oscillation–West Pacific Teleconnection pattern: mature-phase structure and winter impacts. J. Clim. 21 (9), 1979–1997. https://doi.org/10.1175/2007JCLI2048.1.

Lorenz, E.N., 1955. Available potential energy and the maintenance of the general circulation. Tellus 7 (2), 157–167. https://doi.org/10.3402/tellusa.v7i2.8796.

Mantua, N.J., Hare, S.R., Zhang, Y., Wallace, J.M., Francis, R.C., 1997. A pacific interdecadal climate oscillation with impacts on salmon production. Bull. Am. Meteorol. Soc. 78 (6), 1069–1079. https://doi.org/10.1175/1520-0477(1997)078<1069:APICOW>2.0.CO;2.

Mesquita, M.D.S., Hodges, K.I., Atkinson, D.E., Bader, J., 2013. Sea-ice anomalies in the Sea of Okhotsk and the storm track activity in the northern hemisphere. Clim. Dyn. 43 (5–6), 1523–1543. https://doi.org/10.1007/s00382-013-1987-y.

Newman, M., Alexander, M.A., Ault, T.R., Cobb, K.M., Deser, C., Lorenzo, E.D., Mantua, N.J., Miller, A.J., Minobe, S., Nakamura, H., Schneider, N., Vimont, D.J., Phillips, A.S., Scott, J.D., Smith, C.A., 2016. The pacific decadal oscillation, Revisited. J. Clim. 29, 4399–4427. https://doi.org/10.1175/JCLI-D-15-0508.1.

Okajima, S., Nakamura, H., Kuwano-Yoshida, A., Parfitt, R., 2025. Mechanisms for an early spring peak of extratropical cyclone activity in east Asia. J. Clim. 38 (9), 1981–1997. https://doi.org/10.1175/JCLI-D-24-0203.1.

Rayner, N.A., Parker, D.E., Horton, E.B., Folland, C.K., Alexander, L.V., Rowell, D.P., Kent, E.C., Kaplan, A., 2003. Global analyses of sea surface temperature, sea ice, and night marine air temperature since the late nineteenth century. J. Geophys. Res. 108 (D14), 4407. https://doi.org/10.1029/2002JD002670.

Rosenfeld, A., Kak, A.C., 1976. Digital Picture Processing. Academic Press, New York, 457 pp.

Saji, N.H., Goswami, B.N., Vinayachandran, P.N., Yamagata, T., 1999. A dipole mode in the tropical Indian Ocean. Nature 401 (6751), 360–363. https://doi.org/10.1038/43854.

Screen, J.A., 2013. Influence of Arctic sea ice on European summer precipitation. Environ. Res. Lett. 8 (4), 044015. https://doi.org/10.1088/1748-9326/8/4/044015.

Sinclair, M.R., 1997. Objective identification of cyclones and their circulation features in limited-area model simulations. Mon. Weather Rev. 125 (11), 2824–2838. https://doi.org/10.1175/1520-0493(1997)125<2824:OIOCAT>2.0.CO;2.

Thompson, D.W.J., Wallace, J.M., 1998. The arctic oscillation signature in the wintertime observational record. Geophys. Res. Lett. 25 (9), 1297–1300. https://doi.org/10.1029/98GL00950.

Trenberth, K.E., 1997. The definition of el Niño. Bull. Am. Meteorol. Soc. 78 (12), 2771–2777. https://doi.org/10.1175/1520-0477(1997)078<2771:TDOENO>2.0.CO;2.

Vihma, T., 2014. Effects of arctic sea ice decline on weather and climate: a review. Surv. Geophys. 35 (5), 1175–1214. https://doi.org/10.1007/s10712-014-9284-0.

Wallace, J.M., Gutzler, D.S., 1981. Teleconnections in the geopotential height field during the northern hemisphere winter. Mon. Weather Rev. 109 (4), 784–812. https://doi.org/10.1175/1520-0493(1981)109<0784:TITGHF>2.0.CO;2.

Wang, B., Chen, Y., 2014. A new dynamical index for the east Asian winter monsoon. J. Clim. 27 (19), 7430–7445.

Wang, B., Fan, Z., 1999. Choice of South China Sea monsoon index and its relation to ENSO. J. Clim. 12 (4), 994–1004.

Wang, B., He, J., 2012. A dynamical index for the east Asian winter monsoon based on the 500 hPa geopotential height. J. Meteorol. Soc. Jpn. Ser. II 90 (5), 721–736.

Wang, L., Zhang, Y., Li, J., 2013. The western pacific subtropical high in summer: a new index and its physical relationship with the Eurasian teleconnection. J. Clim. 26 (21), 8489–8504.

Webster, P.J., Yang, S., 1992. Monsoon and the predictability of the tropical ocean-atmosphere system. Q. J. R. Meteorol. Soc. 118 (507), 871–921.

Wu, B., Zhang, R., D'Arrigo, R., Su, J., 2013. On the relationship between winter sea ice and summer atmospheric circulation over Eurasia. J. Clim. 26 (15), 5523–5536. https://doi.org/10.1175/JCLI-D-12-00524.1.

Xie, N., Sun, Y., Gao, M., 2020. The influence of five teleconnection patterns on wintertime extratropical cyclones over northwest pacific. Atmosphere 11 (11), 1248. https://doi.org/10.3390/atmos11111248.

Yamashita, Y., Kawamura, R., Iizuka, S., Hatsushika, H., 2012. Explosively developing cyclone activity in relation to heavy snowfall on the Japan Sea side of Central Japan. J. Meteorol. Soc. Jpn. 90 (2), 275–295. https://doi.org/10.2151/jmsj.2012-208.

Yang, S., Kim, K.J., Gong, D.Y., 2002. The east Asian major climate modes and their relationship with the north pacific SST. Geophys. Res. Lett. 29 (23), 2132.

Zhang, J., Xu, H., Ma, J., Deng, J., 2019. Interannual variability of spring extratropical cyclones over the Yellow, Bohai, and East China seas and possible causes. Atmosphere 10 (1), 40. https://doi.org/10.3390/atmos10010040.

Zhang, S., Fu, G., Zhang, Y., Xu, J., Xue, Y., Tang, R., Gao, X., Liu, C., Long, J., 2022. Statistical characteristics and composite environmental conditions of explosive cyclones over the Japan Sea and Kuroshio/Kuroshio extension. Atmosphere 13 (1), 17. https://doi.org/10.3390/atmos13010017.